

Multi-patch/multiple-scattering frequency-time hybrid solver for interior and exterior wave equation problems

Shuai Pan*, Gang Bao[†], Tao Yin[‡] and Oscar P. Bruno[§]

July 9, 2025

Abstract

This paper proposes a new multiple-scattering frequency-time hybrid (FTH-MS) integral equation solver for problems of wave scattering by obstacles in two dimensional space, including interior problems in closed cavities and problems exterior to a set of disconnected open or closed scattering obstacles. The multiple-scattering FTH-MS method is based on a partition of the domain boundary into a user-prescribed set of overlapping open arcs, along with a corresponding sequence of multiple-scattering problems that effectively decompose the interior problem into a series of open-arc wave equation subproblems. The new strategy provides a significant extension of the original FTH-MS algorithm originally presented in [O.P. Bruno, T. Yin, *Math. Comput.* 93(346) (2024) 551-587], in that (1) By allowing for use of an arbitrary number of component arcs, and not just two as in the previous contribution, the new approach affords (1a) A significantly increased geometric flexibility, as well as, (1b) The use of partitions for which each open arc leads to small numbers of iterations if iterative linear-algebra solvers are employed; and, (2) It facilitates parallelization—as the subproblem solutions that are needed at each multiple scattering step can be evaluated in an embarrassingly parallel fashion. Utilizing a suitably-implemented Fourier transformation, each sub-problem is reduced to a Helmholtz frequency-domain problem that is tackled via a uniquely-solvable boundary integral equation. Similar FTH-MS methods are also presented for problems exterior to a number of bounded obstacles. All of the algorithms considered incorporate the previously introduced “time-windowing and recentering” methodology (that enables both treatment of incident signals of long duration and long time simulation), as well as a high-frequency Fourier transform algorithm that delivers numerically dispersionless, spectrally-accurate time evolution for arbitrarily long times.

Keywords: Wave equation, multiple scattering, Fourier transform, integral equation

1 Introduction

We present efficient multi-patch/multiple-scattering frequency-time hybrid algorithms (FTH-MS) for the solution of the time-dependent wave equation in both interior and exterior two-dimensional domains. The proposed methods utilize a multiple scattering strategy that decomposes a given interior time-domain problem into a sequence of limited-duration time-domain problems of scattering by overlapping open arcs, each one of which is reduced (by means of the Fourier transform) to a sequence of Helmholtz frequency-domain problems. As discussed and illustrated in the previous contributions [6, 22], the combined use of frequency-domain boundary-integral solvers and frequency-to-time high-frequency Fourier transform

*School of Mathematical Sciences, University of Electronic Science and Technology of China, Chengdu, Sichuan 611731, China. Email: pans@std.uestc.edu.cn

[†]School of Mathematical Sciences, Zhejiang University, Hangzhou 310027, China. Email: baog@zju.edu.cn

[‡]State Key Laboratory of Mathematical Sciences and Institute of Computational Mathematics and Scientific/Engineering Computing, Academy of Mathematics and Systems Science, Chinese Academy of Sciences, Beijing 100190, China. Email: yintao@lsec.cc.ac.cn

[§]Department of Computing & Mathematical Sciences, California Institute of Technology, 1200 East California Blvd., CA 91125, United States. Email: obruno@caltech.edu

methods results in algorithms that compare well with existing approaches—including methods based on use of volumetric discretizations and temporal time-stepping strategies [11, 30, 31, 36, 47, 48, 50]; as well as methods based on spatio-temporal Green functions and integral equations; and methods based on a combination of a time-discretization and integral equations in the Laplace frequency domain. Indeed, (a) Like other boundary-integral methods, the boundary integral schemes in the FTH-MS algorithm only require discretization of the lower-dimensional domain boundary (thus enabling significant efficiency gains over volumetric methods); and, (b) The combined FTH-MS use of boundary-integral frequency domain solutions and fast and effective high-frequency Fourier transform methods results in essentially spatio-temporally dispersionless algorithms. In particular, (c) Unlike other frequency-time hybrid methods, the FTH-MS algorithm does not incur accumulating temporal dispersion errors and it avoids a certain “infinite-tail” difficulty mentioned below.

The volumetric type approaches, in contrast, generally suffer from spatial and temporal numerical dispersion errors [8] (a problem which can be mitigated [40] if high-order methods are utilized). Thus, for the types of volumetric solvers often used in practice, applications to high-frequency and/or large-time problems typically require the use of fine spatial and temporal meshes—with associated large requirements of computer memory and long computing times. Challenges have also been found in the context of integral equation solvers, including the time-domain boundary integral equation method (TDBIE) [1, 12, 27, 44, 45], which proceeds on the basis of the retarded-potential Green’s function; and the “Convolution Quadrature” method [10, 37, 41] (CQ) which, utilizing a finite-difference time discretization followed by a Laplace-like transformation in discrete time, reduces the original time-domain problem to modified Helmholtz problems over a range of frequencies that can be solved by means of appropriate frequency-domain boundary integral equations (BIE). In particular, the TDBIE method requires integration in challenging domains given by the intersection of the light cone with the overall scattering surface, and it has been found to suffer from numerical instability [12]. As mentioned in [6, Section 2.2.1], on the other hand, the CQ method inherits the dispersive character of the finite-difference approximation that underlies its time discretization, and it gives rise to a challenging infinite tail leading to unbounded memory requirements and increased time-per-timestep as times grow.

The recently introduced frequency-time hybrid (FTH) approach [6] for exterior problems, in contrast, utilizes the Fourier transform to reduce the time-domain problem to sequences of frequency-domain problems for the Helmholtz equation. Relying on a certain “windowing and time-recentering” procedure together with high-frequency Fourier transformation algorithms, the FTH solver can provide highly accurate numerical solutions at low computing costs, with spectral accuracy in time, for problems involving complex scatterers, for incident fields applied over long periods of time, and with extremely low dispersion errors.

The FTH method [6] is not applicable to either interior spatial domains—in which the waves are perpetually trapped, and for which the corresponding interior-domain Helmholtz problems are not uniquely solvable at any frequency k for which $-k^2$ an eigenvalue of the Laplace operator. The recent contribution [22] provides an extension of the FTH applicable to interior spatial domains. The extended method proceeds by exploiting a novel multiple-scattering technique that re-expresses the full time-evolution as a “ping-pong” problem of multiple scattering between two overlapping patches (open-arcs) that cover the domain boundary. As a result, the method [22], which relies on a generalized Huygens-like domain-of-influence condition related to amount of overlap between the two patches, only requires solution of certain *open-arc* frequency-domain scattering problems which are uniquely solvable at all real frequencies. However, since it is limited to decomposing the domain boundary into only two patches, this ping-pong solver may encounter significant difficulties with challenging wave-trapping patches—where iterative frequency-domain solvers often require many iterations. Additionally, the present FTH-MS generalization of the ping-pong multiple scattering algorithm [22] includes a capability to enable the solution of problems of scattering by open arcs—to which the ping-pong solver [22] is not applicable on account of its endpoint singularity-handling approach.

Relying on decompositions of the domain boundary as a union of arbitrary numbers of overlapping arcs, the new FTH-MS method proceeds by adequately accounting for the multiple scattering among all pairs of component arcs: it re-expresses an interior or exterior time-domain problem in terms of a sequence

of open-arc wave equation sub-problems, each of which is solved by means of the FTH solver [6]. We emphasize that, unlike the previous method [22], the new approach can be applied to advantage to open-arc exterior problems as well. By utilizing partitions in terms of sufficiently simple and small open arcs, the new method reduces the overall problem to a number of relatively small frequency domain problems which can be treated effectively and with high accuracy by means of iterative or direct linear-algebra solvers, and which can be parallelized effectively in an embarrassingly parallel fashion.

In a major further improvement, the present contribution eliminates the need for the “smooth extension along normals” singularity-handling technique introduced in [22] to bypass singularities induced by the endpoints of one patch at interior points of neighboring patches; see [22, Fig. 3], the accompanying discussion, and the introductory paragraph of Section 4.3 below. As detailed in Section 4.3, the simplification is achieved by leveraging the structure of the endpoint-induced singularities to design appropriate “smoothing” changes of variables. As a result, the overall approach is significantly streamlined, it is applicable to open-arc exterior problems in addition to the previously considered closed-arc configurations, and is well-suited for potential generalizations to three-dimensional settings.

This paper is organized as follows. Section 2 reviews the basic elements of the FTH solver [6], introduces the necessary Huygens-like domain-of-influence condition, and mentions relevant solution regularity results. Section 3.1 then introduces the main multi-patch multiple scattering concept, and presents the key theoretical result that validates the method: Theorem 3.5. Relying on these ideas, Section 3.2 introduces the multi-patch multiple-scattering FTH-MS algorithm for interior domains, and Section 3.3 extends the method to exterior wave equation problems involving both closed and open scattering obstacles. The computational implementation used is described in Section 4, including, in particular, a study in Section 4.3 which examines the aforementioned end-point and induced singularities, and which introduces variable transformations that remove these singularities and restore high-order accuracy. Numerical examples are presented in Section 5 that illustrate the accuracy and efficiency provided by the proposed methodology.

2 Preliminaries

As a preliminary to the presentation of the multi-patch multiple-scattering FTH-MS solver for interior and exterior wave equation problems, this section briefly lays down the wave problems considered, and it reviews theoretical concepts underlying the exterior and interior FTH-based methods [6, 22]—including the windowing-and-recentering approach [6], the Huygens-like domain-of-influence properties [22] and the regularity properties [9, 23] of the underlying solutions to wave equation problems.

2.1 Interior and exterior wave equation problems

Let $D \subset \mathbb{R}^2$ denote an open domain with a smooth boundary Γ , call $D^e = \mathbb{R}^2 \setminus \overline{D}$ its exterior, and let $u^i(x, t)$ be a given smooth incident field defined for $(x, t) \in \Gamma \times \mathbb{R}$ which vanishes for $t \leq 0$. In this paper we consider the initial and boundary-value problems for the wave equation in both $E = D$ and $E = D^e$, subject to Dirichlet boundary conditions f on Γ ,

$$\begin{cases} \partial_t^2 u(x, t) - c^2 \Delta u(x, t) = 0, & (x, t) \in E \times \mathbb{R}_+, \\ u(x, 0) = \partial_t u(x, 0) = 0, & x \in E, \\ u(x, t) = f(x, t), & (x, t) \in \Gamma \times \mathbb{R}_+, \end{cases} \quad (2.1)$$

where $\mathbb{R}_+ := \{t \in \mathbb{R} : t > 0\}$, $f = -u^i$, and where $c > 0$ and u denote the wave-speed and the scattered field, respectively. Since $u^i(x, t) = 0$ for $t \leq 0$, problem (2.2) can be equivalently written in the form

$$\begin{cases} \partial_t^2 u(x, t) - c^2 \Delta u(x, t) = 0, & (x, t) \in E \times \mathbb{R}, \\ u(x, t) = f(x, t), & (x, t) \in \Gamma \times \mathbb{R}, \end{cases} \quad (2.2)$$

by invoking the causality condition $u(x, t) = 0$ for $x \in E$ and $t \leq 0$. The Dirichlet problem of scattering by an open arc Γ , which is also considered in this paper, can similarly be formulated using equations (2.1) and (2.2) by defining E as the complement of Γ : $E = \Gamma^c$.

Throughout this paper a number of wave-equation problems will be considered which, assuming vanishing boundary data for $t \leq 0$, will be expressed in a form similar to (2.2) in lieu of the equivalent formulation—of the form (2.1)—in terms of vanishing initial conditions at $t = 0$. Throughout this paper a time dependent function will be said to be *causal* if it vanishes for $t \leq 0$.

2.2 FTH solver on the exterior domain $E = D^e$

The FTH solver [6] produces solutions $u(x, t)$ for the exterior domain D^e as indicated in what follows; as mentioned in Section 1, a different approach must be used for the interior domain D on account of a lack of unique solvability for interior Helmholtz problems. For a given time-domain function $g \in L^2(\mathbb{R})$, its Fourier transform, denoted by G , is given by

$$G(\omega) = \mathbb{F}(g)(\omega) := \int_{\mathbb{R}} g(t)e^{i\omega t} dt, \quad \omega \in \mathbb{R}, \quad (2.3)$$

whereas the corresponding inverse Fourier transform \mathbb{F}^{-1} of a frequency-domain function $G \in L^2(\mathbb{R})$ is given by

$$g(t) = \mathbb{F}^{-1}(G)(\omega) := \frac{1}{2\pi} \int_{\mathbb{R}} G(\omega)e^{-i\omega t} d\omega. \quad (2.4)$$

Letting U and F denote the Fourier transforms of the solution u and boundary values f , respectively, it follows that U satisfies the Helmholtz problem with wavenumber $\kappa = \kappa(\omega) = \omega/c \in \mathbb{R}$:

$$\begin{cases} \Delta U(x, \omega) + \kappa^2 U(x, \omega) = 0, & x \in D^e, \\ U(x, \omega) = F(x, \omega), & x \in \Gamma. \end{cases} \quad (2.5)$$

Calling $\Phi_\omega := i/4H_0^{(1)}(\kappa|x-y|)$ the fundamental solution of the Helmholtz equation in \mathbb{R}^2 , letting \mathcal{S}_Γ and \mathcal{D}_Γ denote the frequency-domain single-layer and double-layer potentials

$$\mathcal{S}_\Gamma[\Psi](x, \omega) = \int_{\Gamma} \Phi_\omega(x, y)\Psi(y, \omega)ds_y, \quad (x, \omega) \in D^e \times \mathbb{R}, \quad \text{and} \quad (2.6)$$

$$\mathcal{D}_\Gamma[\Psi](x, \omega) = \int_{\Gamma} \partial_{\nu_y} \Phi_\omega(x, y)\Psi(y, \omega)ds_y, \quad (x, \omega) \in D^e \times \mathbb{R}, \quad (2.7)$$

and introducing the corresponding frequency-domain boundary integral operators

$$V_\Gamma[\Psi](x, \omega) = \int_{\Gamma} \Phi_\omega(x, y)\Psi(y, \omega)ds_y, \quad (x, \omega) \in \Gamma \times \mathbb{R}, \quad (2.8)$$

$$K_\Gamma[\Psi](x, \omega) = \int_{\Gamma} \partial_{\nu_y} \Phi_\omega(x, y)\Psi(y, \omega)ds_y, \quad (x, \omega) \in \Gamma \times \mathbb{R}, \quad (2.9)$$

the frequency-domain solution U can be expressed in the form

$$U(x, \omega) = (\mathcal{D}_\Gamma - i\eta\mathcal{S}_\Gamma)[\Psi](x, \omega), \quad (x, \omega) \in D^e \times \mathbb{R}, \quad (2.10)$$

where Ψ is an unknown density and where η is a given parameter satisfying $\text{Re } \eta \neq 0$. In the limit as $x \rightarrow \Gamma$ the classical frequency-domain combined field integral equation (CFIE)

$$\left(\frac{1}{2}I + K_\Gamma - i\eta V_\Gamma \right) [\Psi](x, \omega) = F(x, \omega), \quad (x, \omega) \in \Gamma \times \mathbb{R} \quad (2.11)$$

results, which is uniquely solvable for all real wavenumbers κ .

The FTH wave equation solver [6] for exterior domains D^e proceeds via effectively performing the following sequence of operations

$$f(x, t) \xrightarrow{\mathbb{F}} F(x, \omega) \xrightarrow{(2.11), (2.10)} U(x, \omega) \xrightarrow{\mathbb{F}^{-1}} u(x, t). \quad (2.12)$$

However, for incident fields u^i and associated boundary data f of long duration, the Fourier transform $F(x, \omega)$ is generally a highly oscillatory function of ω , as a result of the rapidly oscillating factor $e^{i\omega t}$ that appears in the Fourier transform integrand for large values of t —see e.g. [6, Fig. 1]. Under such a scenario a very fine frequency-discretization, requiring $\mathcal{O}(T)$ frequency points, and, thus, a number $\mathcal{O}(T)$ of evaluations of the frequency-domain boundary integral equation solver, is required to obtain the time-domain solution $U(x, t)$. This makes the overall algorithm unacceptably expensive for long-time simulations. To overcome these difficulties, the FTH algorithm [6] relies on a certain “windowing and time-recentering” procedure proposed in [6, Sec. 3.1], that decomposes a scattering problem involving an incident time signal of long duration into a sequence of problems with smooth incident field of a limited duration, all of which can be solved in terms of a fixed set of solutions of the corresponding frequency-domain problems for arbitrarily large values of T .

For a given final time T , the windowing-and-recentering approach is based on use of a smooth partition of unity (POU) $\mathcal{P} = \{\Pi_q(t) \mid q \in \mathcal{Q}\}$, $\mathcal{Q} = \{1, \dots, Q\}$, where the functions Π_q satisfy the relation $\sum_{q \in \mathcal{Q}} \Pi_q(t) = 1$ for $t \in [0, T]$ and, for a certain sequence s_q ($q \in \mathcal{Q}$), each $\Pi_q(t)$ is a non-negative, smooth windowing function of t , supported in the interval $[s_q - H, s_q + H]$ of duration $2H$. Then utilizing the POU \mathcal{P} , any smooth long-time signal $g(t)$, $t \in [0, T]$, can be expressed in the form

$$g(t) = \sum_{q \in \mathcal{Q}} g_q(t), \quad g_q(t) = g(t) \Pi_q(t), \quad (2.13)$$

where g_q is compactly supported in $[s_q - H, s_q + H]$. The corresponding Fourier transform is then given by

$$G(\omega) = \sum_{q \in \mathcal{Q}} G_q(\omega), \quad G_q(\omega) = \int_0^T g_q(t) e^{i\omega t} dt = e^{i\omega s_q} G_{q,slow}(\omega), \quad (2.14)$$

where, defining by

$$\mathbb{F}_{q,slow}(g)(\omega) := \int_{-H}^H g(t + s_q) \Pi_q(t) e^{i\omega t} dt, \quad (2.15)$$

the s_q -centered slow Fourier-transform operator, we call $G_{q,slow}(\omega) = \mathbb{F}_{q,slow}(g)(\omega)$; note that, as suggested by the notation used, $G_{q,slow}$ is a slowly-oscillatory function of ω .

For $q \in \mathcal{Q}$ we now call $F_{q,slow}(x, \omega) = \mathbb{F}_{q,slow}(f)(x, \omega)$ the slow Fourier-transform of the boundary data f , and we let $U_{q,slow}$ be the solution of the Helmholtz equation problem (2.5) with boundary data $F_{q,slow}$. The solution $U_{q,slow}$ can be expressed in the form

$$U_{q,slow}(x, \omega) = (\mathcal{D}_\Gamma - i\eta \mathcal{S}_\Gamma) [\Psi_{q,slow}](x, \omega), \quad (x, \omega) \in D^e \times \mathbb{R}, \quad (2.16)$$

where $\Psi_{q,slow}$ is the unique solution to the frequency-domain CFIE

$$\left(\frac{1}{2} I + K_\Gamma - i\eta V_\Gamma \right) [\Psi_{q,slow}](x, \omega) = F_{q,slow}(x, \omega), \quad (x, \omega) \in \Gamma \times \mathbb{R}. \quad (2.17)$$

It then easily follows that

$$u(x, t) = \mathbb{F}^{-1} \left(\sum_{q \in \mathcal{Q}} e^{i\omega s_q} U_{q,slow} \right) (x, t) = \sum_{q \in \mathcal{Q}} \mathbb{F}^{-1} (U_{q,slow})(x, t - s_q), \quad (x, t) \in D^e \times \mathbb{R}. \quad (2.18)$$

On the basis of an appropriate high-frequency Fourier transform algorithm to produce the Fourier transforms on the right-hand side of (2.18), see [6, Section 4], the FTH solver proceeds via the following sequence of operations

$$f(x, t) \xrightarrow{\mathbb{F}_{q,slow}} F_{q,slow}(x, \omega) \xrightarrow{(2.17),(2.16)} U_{q,slow}(x, \omega) \xrightarrow{(2.18)} u(x, t). \quad (2.19)$$

2.3 Huygens-like domain-of-influence

Like the algorithm [22], the multiple scattering algorithm proposed in this paper depends in an essential manner on a variant of the well known Huygens principle—in a form that is applicable to the problem of scattering by obstacles and open arcs. A Huygens-like domain-of-influence result, which follows by consideration of the properties of the retarded Green function, may be stated as follows.

Theorem 2.1. [41, Proposition 3.6.2] *Let u be the solution to the wave equation problem (2.2). If $f(x, t) = 0$ for all $x \in \Gamma$ and $t \leq t_0$, then for $x \in \mathbb{R}^2 \setminus \Gamma$,*

$$u(x, t) = 0 \quad \text{for all } t \leq t_0 + c^{-1} \text{dist}(x, \Gamma).$$

Remark 2.2. *A version of Theorem 2.1 can also be established for the solution to the wave equation problem*

$$\begin{cases} \partial_t^2 v(x, t) - c^2 \Delta v(x, t) = 0, & (x, t) \in \mathbb{R}^2 \setminus \mathcal{C} \times \mathbb{R}, \\ v(x, t) = g(x, t), & (x, t) \in \mathcal{C} \times \mathbb{R}, \end{cases} \quad (2.20)$$

on the exterior of a bounded Lipschitz open-arc \mathcal{C} .

Theorem 2.1 and its open-arc analog mentioned in Remark 2.2 do not provide sharp time estimates, as they only ensure that the field propagates away from the complete boundary (with speed equal to the speed of sound), but they do not account for propagation along the scattering boundary. In particular, for incident fields illuminating a subset of the boundary of a scatterer, these theoretical results do not establish that the field propagates at the speed of sound along the scattering boundary. To determine the relation between the delay in the arrival of the solution and compactly supported boundary data, a generalized Huygens-like domain-of-influence condition was introduced in [22], which is believed to be valid, which was established rigorously for a flat arc and was demonstrated numerically for curved arcs and closed curves in that reference, but for which a rigorous mathematical proof in the case of general arcs or closed curves is unavailable as yet. In the context of the wave equation problem (2.20) outside the open arc \mathcal{C} , for example, the generalized Huygens-like domain-of-influence condition may be stated as follows.

Condition 2.3. *We say that an open Lipschitz curve \mathcal{C} with endpoints e_1 and e_2 satisfies the restricted Huygens condition iff for every Lipschitz curve $\mathcal{C}^{\text{inc}} \subseteq \mathcal{C}$ satisfying $\text{dist}(\mathcal{C}^{\text{inc}}, \{e_1, e_2\}) > 0$, and for every g defined in \mathcal{C} such that*

$$\{x \in \mathcal{C} \mid g(x, t) \neq 0\} \subseteq \mathcal{C}^{\text{inc}} \quad \text{for all } t > 0, \quad (2.21)$$

the solution $v(x, t)$ to the wave equation problem (2.20) satisfies

$$\{x \in \mathbb{R}^2 \mid v(x, t) \neq 0\} \subseteq \Lambda^s(t) \quad \text{for all } t \leq c^{-1} \text{dist}(\mathcal{C}^{\text{inc}}, \{e_1, e_2\}), \quad (2.22)$$

where

$$\Lambda^s(t) = \{x \in \mathbb{R}^2 \mid \text{dist}(x, \mathcal{C}^{\text{inc}}) \leq ct\}.$$

As in [22], we conjecture that Condition 2.3 holds for arbitrary open and closed Lipschitz curves \mathcal{C} and for all $t > 0$ (even without the restriction $t \leq c^{-1} \text{dist}(\mathcal{C}^{\text{inc}}, \{e_1, e_2\})$). The proof is left for future work. Condition 2.3 expresses a well accepted principle in wave physics, namely, that solutions of the wave equation propagate at the speed of sound, and that the wave field vanishes identically before the arrival of a wavefront. This boundary-propagation character provides a crucial element in the proposed multiple scattering algorithm and, indeed, throughout this paper Condition 2.3 is assumed to be valid.

2.4 Solution regularity

The regularity of the solutions of the wave equation may be described in terms of certain function spaces, as discussed in what follows. For given $\sigma > 0$ and $\alpha, p \in \mathbb{R}$, and for a given Hilbert space K , the spatio-temporal Sobolev spaces $H_{\sigma,\alpha}^p(\mathbb{R}, K)$ of functions with values in K which vanish for $t \leq \alpha$ are defined by [9, 23]

$$H_{\sigma,\alpha}^p(\mathbb{R}, K) := \left\{ f \in \mathcal{L}'_{\sigma,\alpha}(K) : \int_{-\infty+i\sigma}^{\infty+i\sigma} |s|^{2p} \|\mathcal{L}[f](s)\|_K^2 ds < \infty \right\}, \quad (2.23)$$

together with the norm

$$\|f\|_{H_{\sigma,\alpha}^p(\mathbb{R}, K)} := \left(\int_{-\infty+i\sigma}^{\infty+i\sigma} |s|^{2p} \|\mathcal{L}[f](s)\|_K^2 ds \right)^{1/2}, \quad (2.24)$$

where $\mathcal{L}[f]$ denotes the Fourier-Laplace transform of f given by

$$\mathcal{L}[f](s) := \int_{-\infty}^{\infty} f(t) e^{ist} dt, \quad s \in \mathbb{C}_\sigma := \{\omega \in \mathbb{C} : \text{Im}(s) > \sigma > 0\}, \quad (2.25)$$

and where $\mathcal{L}'_{\sigma,\alpha}(K) := \{\phi \in \mathcal{D}'_\alpha(K) : e^{-\sigma t} \phi \in \mathcal{S}'_\alpha(K)\}$ is defined in terms of the sets $\mathcal{D}'_\alpha(K)$ and $\mathcal{S}'_\alpha(K)$ of K -valued distributions and K -valued tempered distributions that vanish for $t \leq \alpha$, respectively. We also call

$$H_\alpha^p(\beta, K) = \{f(x, t)|_{t \in (-\infty, \beta]} : f \in H_{\sigma,\alpha}^p(\mathbb{R}, K)\}$$

the set of all restrictions of functions $f \in H_{\sigma,\alpha}^p(\mathbb{R}, K)$ to the interval $-\infty < t \leq \beta$. It can be checked that, as suggested by the notation used, the space $H_\alpha^p(\beta, K)$ does not depend on σ [22].

Relevant well-posedness results for the problems (2.2) and (2.20) are summarized in the following theorem.

Theorem 2.4. [23, 51] *Let $p \in \mathbb{R}$, $\sigma > 0$ and $\alpha \geq 0$ be given.*

- For $f \in H_{\sigma,\alpha}^p(\mathbb{R}, H^{1/2}(\Gamma))$, the wave equation problem (2.2) admits a unique solution $u \in H_{\sigma,\alpha}^{p-3/2}(\mathbb{R}, H^1(D))$ and $u \in H_{\sigma,\alpha}^{p-3/2}(\mathbb{R}, H_{loc}^1(D^e))$.
- For $g \in H_{\sigma,\alpha}^p(\mathbb{R}, H^{1/2}(\mathcal{C}))$, the wave equation problem (2.20) admits a unique solution $v \in H_{\sigma,\alpha}^{p-3}(\mathbb{R}, H_{loc}^1(\mathbb{R}^2 \setminus \mathcal{C}))$.

3 FTH-MS solver

Reference [22] proposed a novel ‘‘ping-pong’’ multiple scattering algorithm for the solution of time-domain wave scattering problems (2.2) within a closed curve Γ . The ping-pong algorithm proceeds by re-expressing the full time-evolution of the solution u of a boundary-value problem for the wave equation as a problem of multiple scattering between two overlapping subsets (open-arc patches) Γ_1 and Γ_2 of the domain boundary Γ . By appropriately accounting for multiple scattering between Γ_1 and Γ_2 it was shown in [22] that solutions to such open-arc subproblems can be combined to produce a full solution for the given interior domain problem for arbitrarily long time. The present contribution proposes a generalized version of the previous multiple scattering algorithm. In the new setting the full time-evolution of the solution is obtained as the result of a set of multiple scattering processes among arbitrary (user-prescribed) numbers N of overlapping arcs Γ_j (called patches in what follows) whose union equals the domain boundary: $\Gamma = \cup_{j=1}^N \Gamma_j$. Unlike the method [22], the new approach utilizes a POU $\{\chi_j : j = 1, \dots, N\}$ of the domain boundary which is subordinated to the covering of the boundary by the patches Γ_j . (Without loss of generality, this setup assumes a POU in which χ_j is the only POU element that vanishes outside

Γ_j .) While POU's are not used in the algorithm [22], the use of a POU is a key element in the method presented here—which makes it possible to take advantage of the Huygens Condition 2.3 without relying on naturally occurring vanishing boundary values near arc endpoints—a requirement which can easily be ensured in the case of two-arc decompositions, but for which a reasonable generalization to decompositions containing $N > 2$ patches which would additionally be applicable to 2D boundaries in 3D space has not as yet been found. The ability to utilize arbitrary number of patches provides a number of significant benefits, as it enables (i) The development of embarrassingly parallel implementations; (ii) Desirable large reductions in the frequency-domain patch-wise problem sizes required; and, if iterative linear algebra solvers are used for the solution of patch-wise frequency-domain problems, (iii) Significant reductions in the associated number of iterations—as adequately multi-patch decompositions may be designed to avoid wave-trapping patch-wise problems whose solution would typically requires large numbers of iterations.

The basic principles of the new multiple-scattering methods are presented in Section 3.1 in the context of wave problems in an interior domain D . Algorithmic details, once again in the interior-domain context, are presented in Section 3.2, and the theoretical and algorithmic modifications necessary for the treatment of exterior problems are then presented in Section 3.3.

3.1 Multiple-scattering algorithm in the interior domain D

The proposed multiple scattering algorithm for the wave equation problem (2.1) relies on a decomposition of the boundary Γ into a number of overlapping patches. Thus, as illustrated in Figure 1, the scattering surface Γ is covered by a number $N \geq 2$ of overlapping patches $\Gamma_j \subset \Gamma$, $j = 1, \dots, N$, in such a way that $\Gamma = \cup_{j=1}^N \Gamma_j$ and Γ_j has only a non-empty overlap with Γ_{j-1} and Γ_{j+1} (where, for notational convenience, we define $\Gamma_{N+1} = \Gamma_1$ and $\Gamma_0 = \Gamma_N$). In what follows we call $\Gamma_{j,j+1}^{\text{ov}} = \Gamma_j \cap \Gamma_{j+1}$ the overlap of Γ_j and Γ_{j+1} , and we call $\Gamma_j^{\text{tov}} := \Gamma_j \setminus (\Gamma_{j-1,j}^{\text{ov}} \cup \Gamma_{j,j+1}^{\text{ov}})$, $j = 1, \dots, N$, the portion of Γ_j that remains once the regions of overlap with other patches are “truncated”, see Figure 2(a).

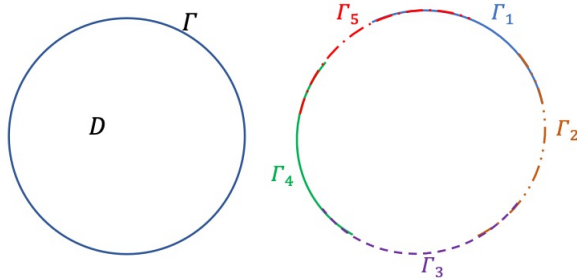


Figure 1: Illustration of the overlapping-patch decomposition of Γ into a number $N = 5$ of overlapping patches.

For each patch Γ_j we introduce a smooth windowing function $\chi_j : \Gamma \rightarrow [0, 1]$ given by

$$\chi_j(x) = \begin{cases} 1, & x \in \Gamma_j^{\text{tov}}, \\ \eta(A_{j,j+1}^{\text{ov}} - d_{j,j+1}^{\text{ov}}(x); c_0 A_{j,j+1}^{\text{ov}}, c_1 A_{j,j+1}^{\text{ov}}), & x \in \Gamma_{j,j+1}^{\text{ov}}, \\ 1 - \eta(A_{j-1,j}^{\text{ov}} - d_{j-1,j}^{\text{ov}}(x); c_0 A_{j-1,j}^{\text{ov}}, c_1 A_{j-1,j}^{\text{ov}}), & x \in \Gamma_{j-1,j}^{\text{ov}}, \\ 0, & x \notin \Gamma_j, \end{cases} \quad j = 1, \dots, N, \quad (3.1)$$

where $0 < c_0 < 1/2 < c_1 < 1$; where $\eta : \mathbb{R} \rightarrow [0, 1]$ is a smooth function equal to 1 for $|t| < t_0$ and equal to 0 for $|t| > t_1$ ($t_1 > t_0$), such as the one given in (3.3) below; and where, for $j = 1, \dots, N$, $A_{j,j+1}^{\text{ov}} := \text{diam}(\Gamma_{j,j+1}^{\text{ov}})$ denotes the diameter of $\Gamma_{j,j+1}^{\text{ov}}$ and $d_{j,j+1}^{\text{ov}}(x)$ denotes the diameter of the arc that connects the point $x \in \Gamma_j$ and the endpoint $x_{j,j+1}$ of Γ_j that is located in the overlap region $\Gamma_{j,j+1}^{\text{ov}}$, see

Figure 2(b). Clearly $\{\chi_j, j = 1, \dots, N\}$ satisfies the POU condition

$$\sum_{j=1}^N \chi_j(x) = 1 \quad \text{for } x \in \Gamma. \quad (3.2)$$

The C^∞ function

$$\eta(t; t_0, t_1) = \begin{cases} 1, & |t| \leq t_0, \\ e^{\frac{2e^{-1/s}}{s-1}}, & t_0 < |t| < t_1, s = \frac{|t|-t_0}{t_1-t_0}, \\ 0, & |t| \geq t_1; \end{cases} \quad (3.3)$$

was utilized to produce all of the numerical results presented in this paper—although, of course, other smooth window functions could be used instead.

We additionally let $\Gamma_j^0 = \{x \in \Gamma_j | \chi_j(x) = 0\}$ and we call $\Gamma_j^{\text{tr}} = \Gamma_j \setminus \Gamma_j^0$ the corresponding truncated portion of Γ_j . The choice of the parameters $0 < c_0 < 1/2 < c_1 < 1$ ensures that

$$\text{dist}\{\Gamma_j^{\text{tr}}, \Gamma \setminus \Gamma_j\} > 0, \quad j = 1, \dots, N;$$

the values $c_0 = 1/3$ and $c_1 = 2/3$ are used throughout this paper. Finally we define the crucial parameter

$$\delta_{\min} = \min_{j=1, \dots, N} \{\text{dist}\{\Gamma_j^{\text{tr}}, \Gamma \setminus \Gamma_j\}\} > 0. \quad (3.4)$$

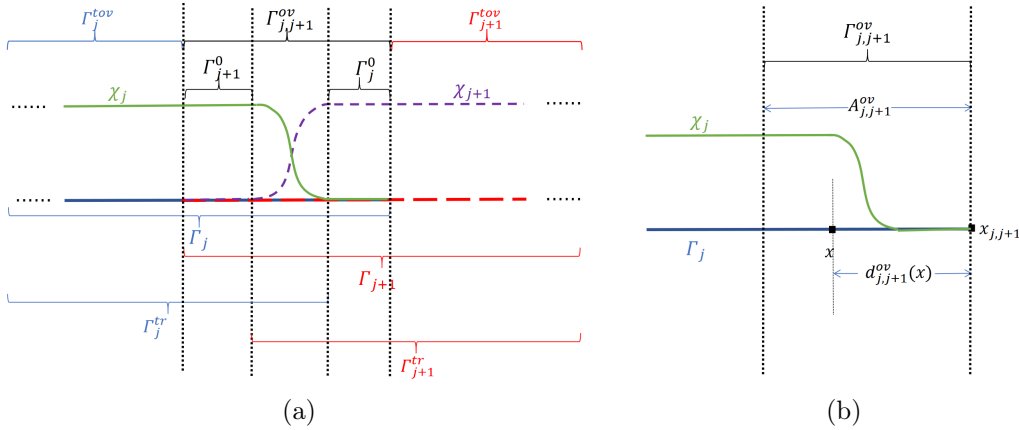


Figure 2: Notations used for the boundary partitioning (a) and windowing functions (b).

Taking into account the finite propagation speed that characterizes the solutions of the wave equation, or, more precisely, the ‘‘Huygens-principle’’ Condition 2.3 introduced in Section 2.3, we propose to produce the solution of the original problem (2.1) in the interior domain D as the sum of wave-equation solutions multiply scattered by the arcs $\Gamma_j, j = 1, \dots, N$. We thus consider the wave equation problems exterior to each arc $\Gamma_j, j = 1, \dots, N$,

$$\begin{cases} \partial_t^2 u_j(x, t) - c^2 \Delta u_j(x, t) = 0, & (x, t) \in \Gamma_j^c \times \mathbb{R}, \\ u_j(x, t) = f_j(x, t), & (x, t) \in \Gamma_j \times \mathbb{R}, \end{cases} \quad (3.5)$$

where $\Gamma_j^c = \mathbb{R}^2 \setminus \Gamma_j$. Theorem 2.4 tells us that, for given $p \in \mathbb{R}$, $\sigma > 0$, $\alpha \geq 0$ and for $f_j \in H_{\sigma, \alpha}^p(\mathbb{R}, H^{1/2}(\Gamma_j))$, the wave equation problem (3.5) admits a unique solution $u_j \in H_{\sigma, \alpha}^{p-3}(\mathbb{R}, H_{loc}^1(\Gamma_j^c))$. The following lemma, whose proof is straightforward, expresses the Condition 2.3 in terms related to the curve $\mathcal{C} = \Gamma_j$ in (3.5) and the complete boundary Γ —and thus presents that Huygens condition in the form in which it will be used in the proof of Theorem 3.5.

Lemma 3.1. Let $p \in \mathbb{R}$, $\sigma > 0$ and $T_0 > 0$, and assume that, for all $j = 1, \dots, N$,

(a) $f_j \in H_{\sigma, T_0}^p(\mathbb{R}, H^{1/2}(\Gamma_j))$ satisfies

$$f_j(x, t) = 0 \quad \text{for } (x, t) \in \Gamma_j^0 \times \mathbb{R}; \quad (3.6)$$

(b) Γ_j satisfies Condition 2.3.

Then, letting $t_0 = \delta_{\min}/c > 0$, and calling $u_j \in H_{\sigma, T_0}^{p-3}(\mathbb{R}, H_{loc}^1(\Gamma_j^c))$ the unique solution of the wave equation problem (3.5), we have

$$u_j(x, t) = 0 \quad \text{for } (x, t) \in (\Gamma \setminus \Gamma_j) \times (-\infty, T_0 + t_0]. \quad (3.7)$$

To describe the proposed multiple-scattering scheme, we use the notational conventions

$$\sum_{k \setminus \{j\}} := \sum_{k=1, k \neq j}^N \quad \text{and} \quad \sum_{k \setminus \{j, j+1\}} := \sum_{k=1, k \neq j, k \neq (j+1)}^N, \quad (3.8)$$

and, for $j = 1, \dots, N$, we inductively define boundary-condition functions $g_{j,m}(x, t)$ ($m \geq 1$) and associated wave-equation solutions $v_{j,m}(x, t)$ ($m \geq 1$) to the problems (3.5) as detailed in what follows.

Definition 3.2. For $m \in \mathbb{N}$, we define $v_{j,m}(x, t)$ to equal the solution $u_j(x, t)$ of the wave equation problem (3.5) with boundary-condition function $f_j = g_{j,m}$ —so that $v_{j,m}$ satisfies the boundary conditions

$$v_{j,m}(x, t) = g_{j,m}(x, t) \quad \text{for } (x, t) \in \Gamma_j \times \mathbb{R}, \quad m \in \mathbb{N}, \quad (3.9)$$

for all $j = 1, \dots, N$, where $g_{j,m}(x, t) : \Gamma_j \times \mathbb{R} \rightarrow \mathbb{C}$ denotes the causal functions defined inductively via the relations

$$g_{j,1}(x, t) = -\chi_j(x) u^i(x, t) \quad (x, t) \in \Gamma_j \times \mathbb{R}, \quad (3.10)$$

and, for $m \geq 1$,

$$g_{j,m+1}(x, t) = -\chi_j(x) \sum_{k \setminus \{j\}} \tilde{v}_{k,j,m}(x, t), \quad (x, t) \in \Gamma_j \times \mathbb{R}. \quad (3.11)$$

Here, for $j = 1, \dots, N$, $(x, t) \in \Gamma_j \times \mathbb{R}$, $k = 1, \dots, N, k \neq j$, and $m \geq 1$, $\tilde{v}_{k,j,m}(x, t)$ denotes the function

$$\tilde{v}_{k,j,m}(x, t) = \begin{cases} v_{k,m}(x, t), & x \in \Gamma_j, k \notin \{j-1, j+1\}, \\ v_{k,m}(x, t), & x \in \Gamma_j \setminus \Gamma_k, k = j-1 \text{ and } k = j+1, \\ 0, & x \in \Gamma_{j-1, j}^{\text{ov}}, k = j-1, \\ 0, & x \in \Gamma_{j, j+1}^{\text{ov}}, k = j+1. \end{cases} \quad (3.12)$$

Remark 3.3. The definition of the windowing function χ_j ($j = 1, \dots, N$) ensures that

$$g_{j,m}(x, t) = 0 \quad \text{for } (x, t) \in \Gamma_j^0 \times \mathbb{R}, \quad j = 1, \dots, N, \quad m \in \mathbb{N}, \quad (3.13)$$

which is a crucial property in the proposed multiple scattering algorithm—in that it ensures that the solution of the problem of scattering by the open arc Γ_j with boundary conditions given by the incident field $g_{j,m}$ coincides, at least for a certain time interval, with the solution of the problem of scattering by the complete surface Γ , with incident field equal to $g_{j,m}$ for $x \in \Gamma$. Moreover, the function $g_{j,m}(x, t)$ is continuous and vanishes at the endpoints of Γ_j^{tov} , despite the seemingly discontinuous nature of the closely related definition (3.12) at those points. The claimed continuity of $g_{j,m}(x, t)$ holds since, for $m \geq 2$ and $k = j \pm 1$, $g_{k,m}(x, t)$ is continuous and vanishes at the endpoints of Γ_j^{tov} for all $t \in \mathbb{R}$ (as it follows from the definitions (3.10)–(3.11) with $j = k$), which implies that $v_{k,m}$, and, thus, $\tilde{v}_{k,j,m}(x, t)$, tend to zero, for all $t \in \mathbb{R}$, as x approaches the endpoints of Γ_j^{tov} .

We now consider the $M \times N$ -th order multiple-scattering sum

$$u_M(x, t) := \sum_{m=1}^M \sum_{j=1}^N v_{j,m}(x, t), \quad (3.14)$$

which includes contributions from all $M \times N$ “ping-pong” scattering iterates $v_{j,m}(x, t)$ with $j = 1, \dots, N$, $m = 1, \dots, M$. Theorem 3.5 below establishes that, throughout D , the multiple-scattering sum u_M coincides with the exact solution u of the original wave equation problem (2.1) for $t \leq T(M)$, where, for $M \in \mathbb{N}$ we define

$$T(M) = M\delta_{\min}/c. \quad (3.15)$$

The proof of Theorem 3.5 relies on certain relations, established in the following lemma, concerning the solutions $v_{j,m}$ and the boundary value functions $g_{j,m}$ introduced in Definition 3.2.

Lemma 3.4. *With reference to equation (3.15), for each $M \in \mathbb{N}$ and each integer j , $1 \leq j \leq N$, the relations*

$$v_{j,M}(x, t) + \sum_{m=1}^{M-1} \sum_{k=1}^N v_{k,m}(x, t) + u^i(x, t) = 0, \quad (x, t) \in \Gamma_j^{\text{tov}} \times \mathbb{R}, \quad (3.16)$$

$$v_{j,M}(x, t) + v_{j\pm 1, M}(x, t) + \sum_{m=1}^{M-1} \sum_{k=1}^N v_{k,m}(x, t) + u^i(x, t) = 0, \quad (x, t) \in (\Gamma_j \cap \Gamma_{j\pm 1}) \times \mathbb{R}, \quad \text{and} \quad (3.17)$$

$$g_{j,M}(x, t) = 0, \quad (x, t) \in \Gamma_j \times (-\infty, T(M-1)] \quad (3.18)$$

are satisfied.

Proof. We establish (3.16) through (3.18) by induction in M . In the case $M = 1$, (3.16) follows directly from (3.9) and (3.10); equation (3.17) results once again from (3.9) and (3.10) together with (3.1) and (3.2); and (3.18) follows from (3.10) since $u^i \in H_{\sigma,0}^p(\mathbb{R}, H^{1/2}(\partial D))$ and, thus, vanishes for $t \leq 0$ (Section 2.4). Having established (3.16) through (3.18) for $M = 1$, the corresponding inductive steps are considered next.

Let $L \in \mathbb{N}$ and assume (3.16) holds for $M = L$ and $1 \leq j \leq N$. Then, the validity of (3.16) with $M = L + 1$ is equivalent to the validity of the relation

$$v_{j,L+1}(x, t) + \sum_{k \setminus \{j\}} v_{k,L}(x, t) = 0, \quad (x, t) \in \Gamma_j^{\text{tov}} \times \mathbb{R}, \quad (3.19)$$

which results as the difference between the $M = L + 1$ and the $M = L$ versions of (3.16). But, in view of (3.9) and (3.12) and since $\chi_j(x) = 1$ for $x \in \Gamma_j^{\text{tov}}$, (3.19) coincides with (3.11) for $(x, t) \in \Gamma_j^{\text{tov}} \times \mathbb{R}$ and therefore holds true. The proof of (3.16) for $M \in \mathbb{N}$ is thus complete.

We next consider the inductive step for (3.17) with a “+” sign; the relation with a “−” sign follows similarly. Let us thus assume the +-sign version of (3.17) holds for $M = L$ for a given $L \in \mathbb{N}$ and for $1 \leq j \leq N$. The validity of the +-sign version of (3.17) for $M = L + 1$ is equivalent to the validity of the relation

$$v_{j,L+1} + v_{j+1,L+1} + \sum_{k \setminus \{j,j+1\}} v_{k,L}(x, t) = 0, \quad (x, t) \in \Gamma_{j,j+1}^{\text{ov}} \times \mathbb{R}, \quad (3.20)$$

that results as the difference between the $M = L + 1$ and the $M = L$ +-sign relations. But, in view of (3.9) and (3.11) and using the notations (3.8), the relation (3.20) may be re-expressed in the form $-\chi_j(x) \sum_{k \setminus \{j\}} \tilde{v}_{k,j,L}(x, t) - \chi_{j+1}(x) \sum_{k \setminus \{j+1\}} \tilde{v}_{k,j+1,L}(x, t) + \sum_{k \setminus \{j,j+1\}} v_{k,L}(x, t) = 0$. Using all four expressions in (3.12) for the case $x \in \Gamma_{j,j+1}^{\text{ov}}$ considered presently, in turn, the latter relation is equivalent to $-\chi_j(x) \sum_{k \setminus \{j,j+1\}} v_{k,j,L}(x, t) - \chi_{j+1}(x) \sum_{k \setminus \{j,j+1\}} v_{k,j+1,L}(x, t) + \sum_{k \setminus \{j,j+1\}} v_{k,L}(x, t) = 0$ —which clearly holds true in view of (3.1) and (3.2). The proof of (3.17) is thus complete.

We finally consider the inductive step for (3.18): assuming this relation holds for $M = L \in \mathbb{N}$ and for $1 \leq j \leq N$, we seek to establish its $M = L + 1$ version which, in view of (3.11), may equivalently be expressed in the form

$$-\chi_j(x) \sum_{k \setminus \{j\}} \tilde{v}_{k,j,L}(x,t) = 0 \quad \text{on } \Gamma_j \times (-\infty, T(L)]. \quad (3.21)$$

To establish (3.21), using (3.9), (3.12) and the inductive hypothesis we show that each term $\tilde{v}_{k,j,L}(x,t)$ in the sum (3.21) vanishes for $(x,t) \in \Gamma_j \times (-\infty, T(L)]$, and we do this for each one of the two cases $k = j \pm 1$ and $k \neq j \pm 1$. In the first case, and restricting attention to the subcase $k = j + 1$ (since the subcase $k = j - 1$ follows similarly) we see from (3.12) that $\tilde{v}_{j+1,j,L}(x,t) = 0$ for $(x,t) \in \Gamma_{j,j+1}^{\text{ov}} \times \mathbb{R}$, and $\tilde{v}_{j+1,j,L}(x,t) = v_{j+1,L}(x,t)$ for $(x,t) \in (\Gamma_j \setminus \Gamma_{j+1}) \times \mathbb{R}$, so that, for the $k = j + 1$ subcase considered presently, it only remains to show that $v_{j+1,L}(x,t) = 0$ for $(x,t) \in (\Gamma_j \setminus \Gamma_{j+1}) \times (-\infty, T(L)]$. But, in view of (3.9) we have $v_{j+1,L}(x,t) = g_{j+1,L}(x,t)$ for $(x,t) \in \Gamma_{j+1} \times \mathbb{R}$, and, thus (i) $v_{j+1,L}(x,t) = 0$ for $(x,t) \in \Gamma_{j+1} \times (-\infty, T(L-1)]$ (since $g_{j+1,L}(x,t) = 0$ for $(x,t) \in \Gamma_{j+1} \times (-\infty, T(L-1)]$ by the $M = L$ inductive hypothesis); and (ii) $v_{j+1,L}(x,t) = 0$ for $(x,t) \in \Gamma_{j+1}^0 \times \mathbb{R}$ (since, on account of the $\chi_{j+1}(x)$ factor in (3.11) we have $g_{j+1,L}(x,t) = 0$ for $(x,t) \in \Gamma_{j+1}^0 \times \mathbb{R}$). The conclusions in the points (i) and (ii) just considered enable us to invoke Lemma 3.1 with j replaced by $j + 1$, and, thus, to ascertain that $v_{j+1,L}(x,t) = 0$ for $(x,t) \in (\Gamma_j \setminus \Gamma_{j+1}) \times (-\infty, T(L)]$ —which concludes the proof in the case $k = j \pm 1$. In the case $k \neq j \pm 1$, finally, by (3.12) we have $\tilde{v}_{k,j,L}(x,t) = v_{k,L}(x,t)$, and the proof follows by invoking Lemma 3.1 once again, on the basis of the inductive hypothesis (which tells us that $v_{k,L}(x,t) = g_{k,L}(x,t) = 0$ for $(x,t) \in \Gamma_k \times (-\infty, T(L-1)]$), together with the fact that $\text{dist}(\Gamma_k, \Gamma_j) \geq \delta_{\min}$, to conclude that $\tilde{v}_{k,j,L}(x,t) = v_{k,L}(x,t) = 0$ for $(x,t) \in \Gamma_j \times (-\infty, T(L)]$, as needed. The proof of the lemma is now complete. \square

Theorem 3.5. *Let $M \in \mathbb{N}$, $p \in \mathbb{R}$ and $\sigma > 0$. Then, with reference to equation (3.8), for given $u^i \in H_{\sigma,0}^p(\mathbb{R}, H^{1/2}(\Gamma))$ we have $u_M \in H_0^{p-3/2}(T(M), H^1(D))$, and the solution u of the problem (2.2) with $E = D$ (interior problem) is given by*

$$u(x,t) = u_M(x,t) \quad \text{for } (x,t) \in D \times (-\infty, T(M)]. \quad (3.22)$$

Proof. The fact that $u_M \in H_0^{p-3/2}(T(M), H^1(D))$ follows as in the proof of [22, Theorem 2.8]. In view of the uniqueness of solution to equation (3.5), to establish (3.22) it suffices to show that for all $M \in \mathbb{N}$, the function u_M satisfies the boundary conditions

$$u_M(x,t) + u^i(x,t) = 0 \quad \text{for } (x,t) \in \Gamma \times (-\infty, T(M)], \quad (3.23)$$

or, equivalently, since $\Gamma = \cup_{j=1}^N \Gamma_j$, that

$$u_M(x,t) + u^i(x,t) = 0 \quad \text{for } (x,t) \in \Gamma_j \times (-\infty, T(M)] \quad \text{and } 1 \leq j \leq N. \quad (3.24)$$

Noting that

$$u_M(x,t) = \sum_{k=1}^N v_{k,M}(x,t) + \sum_{m=1}^{M-1} \sum_{k=1}^N v_{k,m}(x,t), \quad (3.25)$$

in what follows we establish (3.24) for a given j ($1 \leq j \leq N$) by separately considering (3.25) in the cases $(x,t) \in \Gamma_j^{\text{tov}} \times (-\infty, T(M)]$ and $(x,t) \in (\Gamma_j \cap \Gamma_{j \pm 1}) \times (-\infty, T(M)]$.

In order to verify (3.24) for a given j and for $(x,t) \in \Gamma_j^{\text{tov}} \times (-\infty, T(M)]$ we first note that since we have $g_{k,M}(x,t) = 0$ for $(x,t) \in \Gamma_k \times (-\infty, T(M-1))$ (in view of (3.18)) and $g_{k,M}(x,t) = 0$ for $(x,t) \in \Gamma_k^0 \times \mathbb{R}$ (in view of (3.13)), and in consideration of (3.9), Lemma 3.1 tells us that, for $k \neq j$, $v_{k,M}(x,t) = 0$ for $(x,t) \in (\Gamma_j \setminus \Gamma_k) \times (-\infty, T(M)]$. Applying this relation for $k = j \pm 1$ we conclude that

$$v_{j \pm 1, M}(x,t) = 0 \quad \text{for } (x,t) \in \Gamma_j^{\text{tov}} \times (-\infty, T(M)], \quad (3.26)$$

while applying it for other values of k we obtain

$$v_{k, M}(x,t) = 0 \quad \text{for } k \notin \{j-1, j, j+1\} \quad \text{and } (x,t) \in \Gamma_j \times (-\infty, T(M)]. \quad (3.27)$$

In view of (3.26) and (3.27), equation (3.25) reduces to

$$u_M(x, t) = v_{j,M}(x, t) + \sum_{m=1}^{M-1} \sum_{k=1}^N v_{k,m}(x, t) \quad \text{for } (x, t) \in \Gamma_j^{\text{tov}} \times (-\infty, T(M)], \quad (3.28)$$

and it reduces to

$$u_M(x, t) = v_{j,M}(x, t) + v_{j\pm 1,M}(x, t) + \sum_{m=1}^{M-1} \sum_{k=1}^N v_{k,m}(x, t) \quad \text{for } (x, t) \in \Gamma_j \cap \Gamma_{j\pm 1} \times (-\infty, T(M)]. \quad (3.29)$$

The desired relation (3.23) now follows directly from (3.28) and (3.29) in view of (3.16) and (3.17), and the proof is thus complete. \square

3.2 FTH-MS solver: interior problem

The procedure embodied in Definition 3.2, Lemma 3.4 and Theorem 3.5 can readily be implemented, on the basis of the methods described in Section 2.2 and [22], as an effective methodology for the solution of the problem (2.2) with $E = D$ (interior problem); the resulting interior FTH-MS algorithm is described in what follows. Using the notations introduced in Section 2.2, for $m \in \mathbb{N}$, $j = 1, \dots, N$ and $q \in \mathcal{Q}$ we call $G_{j,m,q}(x, \omega) = \mathbb{F}_{q, \text{slow}}(g_{j,m})(x, \omega)$ the slow Fourier-transform of the boundary data $g_{j,m}$, and we let $V_{j,m,q}$ denote the solution to the Helmholtz equation problem in Γ_j^c with Dirichlet boundary data $G_{j,m,q}$ on Γ_j . The solution $V_{j,m,q}$ is expressed in the form

$$V_{j,m,q}(x, \omega) = \mathcal{S}_{\Gamma_j}[\Psi_{j,m,q}](x, \omega), \quad (x, \omega) \in \Gamma_j^c \times \mathbb{R}, \quad (3.30)$$

(equation (2.6) but with $(x, \omega) \in \Gamma_j^c \times \mathbb{R}$), where, using (2.8), $\Psi_{j,m,q} \in \tilde{H}^{-1/2}(\Gamma_j)$ denotes the unique solution of the frequency-domain BIE

$$V_{\Gamma_j}[\Psi_{j,m,q}](x, \omega) = G_{j,m,q}(x, \omega), \quad (x, \omega) \in \Gamma_j \times \mathbb{R}, \quad (3.31)$$

see e.g. [43]. The solution $v_{j,m}$ is then given by

$$v_{j,m}(x, t) = \mathbb{F}^{-1} \left(\sum_{q \in \mathcal{Q}} e^{i\omega s_q} V_{j,m,q} \right) (x, t) = \sum_{q \in \mathcal{Q}} \mathbb{F}^{-1} (V_{j,m,q})(x, t - s_q), \quad (x, t) \in \Gamma_j^c \times \mathbb{R}. \quad (3.32)$$

Using these results, notations and conventions, the proposed FTH-MS method for the interior problem (2.2) is presented in what follows (Algorithm 1). Here and throughout this paper, the symbol sequence “+=” denotes the binary assignment operator commonly used in C++ and other programming languages, which adds the value of the right operand to the value of the left operand, and then assigns the result back to the left operand.

Remark 3.6. *The patches Γ_j should be specifically chosen to be nontrapping, since, as detailed in Remarks 3.7 and 3.8, the use of such type of patches significantly impacts the efficiency of the algorithm.*

Remark 3.7. *Although Algorithm 1, per its line 12, evaluates $u_M(x, t)$ as a sum of an increasing number of terms as t and M grow, the selection of non-trapping patches Γ_j ensures the rapid decay of the solutions $v_{j,m}(x, t)$ as t increases—at least for the cases considered in this paper, where the 2D incident signal consists entirely of frequency components at nonzero frequencies. In such cases, integration by parts arguments similar to the 3D treatment [5] can be used to establish fast solution decay. As a result of this rapid decay, the total number of active terms $v_{j,m}(x, t)$ in the algorithm’s line 12 (i.e., those exceeding a given error tolerance $\varepsilon^{\text{tol}} > 0$) remains asymptotically close to a fixed integer over time. Consequently, the computational cost per unit time remains uniformly bounded as time grows. In cases for which the incident signal includes frequency content at zero frequency the frequency-asymptotic methods presented in [7] could be applied in the present context to ensure, once again, uniformly bounded computing times as time grows.*

Algorithm 1 FTH-MS solver for the problem (2.2) in interior domains

- 1: Initialize $u_M(x, t) = 0, (x, t) \in E \times [0, s_Q]$.
 - 2: Do $m = 1, 2, \dots, M$
 - 3: Do $j = 1, 2, \dots, N$
 - 4: Evaluate the boundary data $g_{j,m}(x, t), (x, t) \in \Gamma_j \times [0, s_Q + H]$ via relations (3.10)-(3.11).
 - 5: Set $v_{j,m}(x, t) = 0, (x, t) \in \bar{E} \times [0, s_Q + H]$.
 - 6: Do $q = 1, 2, \dots, Q$
 - 7: Evaluate the boundary data $G_{j,m,q}(x, \omega) = \mathbb{F}_{q,slow}(g_{j,m})(x, \omega), (x, \omega) \in \Gamma_j \times \mathbb{R}$.
 - 8: Solve the integral equations (3.31) with solution $\Psi_{j,m,q}$.
 - 9: Compute $V_{j,m,q}(x, \omega), (x, \omega) \in \Gamma_j^c \times \mathbb{R}$ using equation (3.30).
 - 10: Compute $v_{j,m}(x, t) += \mathbb{F}^{-1}(V_{j,m,q})(x, t - s_q), (x, t) \in \bar{E} \times [0, s_Q + H]$.
 - 11: End Do
 - 12: Compute $u_M(x, t) += v_{j,m}(x, t), (x, t) \in E \times [0, s_Q]$ per equation (3.14) (see Remark 3.7).
 - 13: End Do
 - 14: End Do
-

Remark 3.8. *The use of non-trapping patches Γ_j offers a significant computational advantage when iterative linear algebra algorithms are employed to obtain the required frequency-domain solutions. Specifically, the number of iterations required for an iterative algorithm to solve the integral equations (3.31) on non-trapping patches is considerably lower than that required for solving the corresponding equations on trapping curves; see Figure 16.*

3.3 FTH-MS solver: exterior problem

The methods introduced in Sections 3.1 and 3.2, including Theorem 3.5, can be extended with minimal modifications to apply to the wave equation (2.2) in an exterior domain E , including scenarios where the boundary $\Gamma = \partial E$ consists of a combination of open and closed curves. Using this strategy, the implementation of the exterior FTH-MS solver involves decomposing each connected component of the curve boundary Γ into a union of overlapping open arcs, as described in Section 3.2. This approach is particularly beneficial when the curves induce trapping, as discussed in Remark 3.6. As part of this treatment, the necessary frequency-domain solutions are obtained through equations (3.30) and (3.31).

If preferable, however, boundary-connected components that are closed curves can be treated as a single patch Γ_j , and in that case the necessary frequency-domain solutions $V_{j,m,q}$ (cf. Section 3.2) are obtained in the form

$$V_{j,m,q}(x, \omega) = (\mathcal{D}_{\Gamma_j} - i\eta\mathcal{S}_{\Gamma_j}) [\widehat{\Psi}_{j,m,q}](x, \omega), \quad (x, \omega) \in D_j^c \times \mathbb{R}. \quad (3.33)$$

Here, defining $G_{j,m,q}$ as in Section 3.2, $\Psi_{j,m,q} \in H^{1/2}(\Gamma_j)$ denotes the unique solution of the frequency-domain CFIE

$$\left(\frac{1}{2}I + K_{\Gamma_j} - i\eta V_{\Gamma_j} \right) [\widehat{\Psi}_{j,m,q}](x, \omega) = G_{j,m,q}(x, \omega), \quad (x, \omega) \in \Gamma_j \times \mathbb{R}; \quad (3.34)$$

cf. Section 2.2. The FTH-MS algorithm then proceeds as in the interior domain case considered in the previous section. In all numerical examples in this paper that include closed curves as connected boundary components, these curves are treated using the CFIE equation, as outlined above.

4 Computational implementation

The numerical implementations of both the interior-domain Algorithm 1 and the exterior-domain counterpart outlined in Section 3.3 require the evaluation of Fourier transforms, layer potentials, and boundary integral operators. The next two subsections summarize the strategies employed for these computations.

4.1 High-frequency Fourier transform methods

The Fourier transformation procedures we use coincide with those proposed in [6]. They rely on the fact that if $g(t)$ and $G(\omega)$ are smooth functions that decay superalgebraically—i.e., faster than any negative power of t and ω , respectively, as these variables tend to $\pm\infty$ —then the error in the truncated Fourier-transform approximation

$$g(t) \approx \frac{1}{2\pi} \int_{-W}^W G(\omega) e^{-i\omega t} d\omega \quad (4.1)$$

of the exact transform (2.4), as well as the error in the corresponding forward transform of $g(t)$ truncated to the interval $[-T, T]$, both decay superalgebraically as $W \rightarrow \infty$ and $T \rightarrow \infty$, respectively. Consequently, the needed Fourier transform (4.1) and related time-truncated inverse Fourier transform can be evaluated by means of the high-frequency quadrature methods [22, Secs. 3 and 4], respectively, with errors that decay superalgebraically fast as both the integration intervals and the number of quadrature points are increased.

In the 2D context, in particular, owing to the fact that the 2D frequency-domain solutions generally contains integrable $\mathcal{O}(\log|\omega|)$ singularities, the evaluation of the corresponding Fourier transforms with high-order accuracy requires special considerations. In detail, in the 2D case the approximate inverse Fourier transform integrals (4.1) are expressed in the form

$$g(t) \approx \frac{1}{2\pi} \left(\int_{-W}^{-w_c} + \int_{-w_c}^{w_c} + \int_{w_c}^W \right) G(\omega) e^{-i\omega t} d\omega, \quad (4.2)$$

which may be further decomposed into 1) Integrals of the form

$$I_a^b[G](t) = \int_a^b G(\omega) e^{-i\omega t} d\omega, \quad (4.3)$$

where G is a smooth non-periodic function; and, 2) Half-interval integrals

$$I_0^{w_c}[G](t) = \int_0^{w_c} G(\omega) e^{-i\omega t} d\omega \quad \text{and} \quad I_{-w_c}^0[G](t) = \int_{-w_c}^0 G(\omega) e^{-i\omega t} d\omega, \quad (4.4)$$

where $G(\omega)$ contains a logarithmic singularity at $\omega = 0$. The regular integral $I_a^b[G](t)$ can be evaluated by expressing the non-periodic function $G(\omega)$, $\omega \in [w_c, W]$ as a Fourier-continuation trigonometric polynomial [4, 6, 19] and subsequent explicit term-wise integration. To treat the integral $I_0^{w_c}[G](t)$, which involves a logarithmic singularity at $\omega = 0$, at fixed cost for arbitrarily large times t , a modified ‘‘Filon-Clenshaw-Curtis’’ high-order quadrature approach was developed in [6] by introducing a graded set

$$\left\{ \mu_j = w_c \left(\frac{j}{P} \right)^p, j = 1, \dots, P \right\},$$

of points in the interval $(0, w_c)$ and associated integration sub-intervals (μ_j, μ_{j+1}) , $j = 1, \dots, P$, on each one of which the integral $I_{\mu_j}^{\mu_{j+1}}[G](t)$ is produced by means of the Clenshaw-Curtis quadrature rule. The Fourier transform

$$\mathbb{F}_{q,slow}(g)(\omega) := \int_{-H}^H g(t + s_q) \Pi_q(t) e^{i\omega t} dt$$

for smooth boundary-values function g , finally, can be obtained in a manner analogous to that used for the evaluation of $I_{w_c}^W[G](t)$ except that, on account of the use of compactly supported windowing function Π_q , the integrand may be viewed as a periodic function and, thus, a regular Fourier expansion of the function $g(t + s_q) \Pi_q(t)$, $t \in [-H, H]$ may be used, instead of a the Fourier continuation used for $I_{w_c}^W[G](t)$.

4.2 Single- and double-layer potentials on closed curves and open arcs

The numerical implementation of the FTH-MS algorithm also requires evaluating and inverting specific integral operators, as well as computing certain layer potentials, both of which are associated with the curves Γ_j , for $j = 1, \dots, N$. These curves may be either closed or open; in the following, we discuss the corresponding algorithms for each case. For each closed curve Γ_j , the relevant integral operators and layer potentials include \mathcal{S}_{Γ_j} and \mathcal{D}_{Γ_j} , as well as V_{Γ_j} and K_{Γ_j} , which are given in equations (3.33) and (3.34), respectively. For each open arc Γ_j , in turn, the required integral operators and layer potentials include \mathcal{S}_{Γ_j} and V_{Γ_j} , as given in equations (3.30) and (3.31), respectively. All of these operators can be expressed in the form

$$\mathcal{H}_j(x, \omega) = \int_{\Gamma_j} \Psi_\omega(x, y) \psi_j(y, \omega) ds_y, \quad x \in \Gamma_j \text{ or } x \in \mathbb{R}^2 \setminus \Gamma_j, \quad (4.5)$$

where Ψ_ω equals either Φ_ω or $\partial_{\nu_y} \Phi_\omega$ and where $\psi_j(y, \omega)$ represents the integral density function.

In the implementations used in this paper, both closed-curve and open-arc integrals of the form (4.5) are evaluated numerically using spectral representations of the density function ψ_j . For closed curves, these integrals are computed with high accuracy using the well-established Nyström method [24]. The treatment of open arcs, however, requires more detailed considerations; for clarity, those details are provided separately in Section 4.3. Additionally, as part of the FTH-MS method, the singular integrals (4.5) must be evaluated at a sufficiently large number of frequency discretization points ω within the interval $[-W, W]$. To reduce the computational cost, an appropriate decomposition of the singular kernel is employed, as described in [22, Section 3.2], and we refer to that source for further details in this regard.

4.3 Frequency-domain FTH-MS open-arc problems: additional singularities

The proposed FTH-MS algorithm evaluates the integrals in (4.5) using open-arc techniques introduced in [18] and [21], but in a modified form that accounts for the unique singularity structure in the FTH-MS open-arc density functions ψ_j . While the densities ψ_j exhibit endpoint singularities analogous to those observed in classical open-arc problems, they also feature additional “induced” singularities due to the overlaps between Γ_j and $\Gamma_{j\pm 1}$, as described in what follows. (As discussed in Section 1, the previous contribution [22] employs a “smooth extension along normals” technique that, while effectively eliminating all induced singularities through geometric modifications, is somewhat cumbersome, is not applicable to open-arc scatterers, and does not generalize effectively to the three-dimensional context.) Before considering the special FTH-MS open-arc singularities, however, we provide some background on density singularities and numerical methods in the context of related problems of scattering by a single smooth open arc $\tilde{\Gamma}$ under illumination by a smooth incident field, with Dirichlet boundary conditions, as considered in [18] and [21].

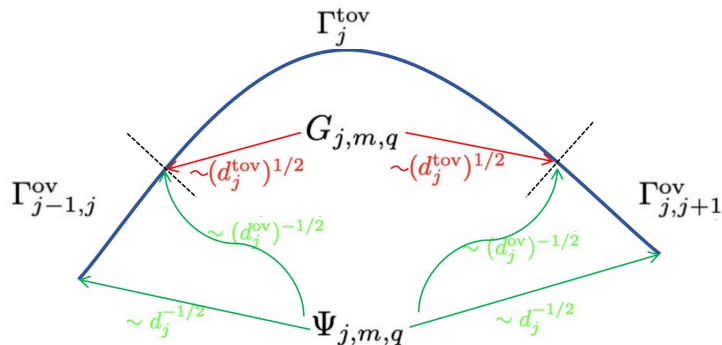


Figure 3: Singularities of the functions $G_{j,m,q}$ and $\Psi_{j,m,q}$ on the arc $\Gamma_j = \Gamma_{j-1,j}^{\text{ov}} \cup \Gamma_j^{\text{tov}} \cup \Gamma_{j,j+1}^{\text{ov}}$.

Considering such “smooth illumination” Dirichlet problems, the approach [18] addresses the singular nature of the associated density $\tilde{\psi}$ at the endpoints of $\tilde{\Gamma}$ by expressing the density in the form

$$\tilde{\psi} = \frac{\alpha}{w}, \quad (4.6)$$

where α is a smooth density function, and where w is a fixed function that, near each endpoint of $\tilde{\Gamma}$, equals the product of a smooth non-vanishing function and the square-root of the distance to the endpoint. This formulation captures the singularity in the density $\tilde{\psi}$ while ensuring that the density function α remains smooth near the endpoints. Reference [18] accurately computes the necessary single-layer integrals by means of a spectral discretization of the density α over the entire arc. In this paper we leverage the 2D Chebyshev-based rectangular-polar spectral discretization method [21, 22] instead. This method not only explicitly accounts for the endpoint singularity (4.6), but it also enables the arc to be partitioned into a prescribed number of non-overlapping “integration patches.” This partitioning greatly enhances the generality and flexibility of the overall methodology, providing, in particular, significant advantages in the context of the FTH-MS algorithm.

As mentioned earlier and as detailed in what follows, additional singularities emerge in the open-arc problems associated with the FTH-MS method. For clarity we present the description within the framework of the interior problem considered in Section 3.2, and using the notation introduced in that section. (The corresponding concepts and algorithms required for the exterior problem presented in Section 3.3 are entirely analogous.) Thus, using the notations in Section 3.2 we note that, as a result of the overlapping-arc decompositions used as part of the FTH-MS framework, the endpoint singularities of the arc Γ_j introduce corresponding singularities in the arcs $\Gamma_{j\pm 1}$ since, by construction, the endpoints of Γ_j are contained within $\Gamma_{j-1} \cup \Gamma_{j+1}$.

In detail, we note that, per Remark 3.3, the boundary functions $g_{j,m}$ with $m > 1$, and, hence, the functions $G_{j,m,q}$ with $m > 1$, are continuous and vanish at the endpoints of Γ_j^{tov} . However, it can be checked that the singularities of the densities $\psi_{j\pm 1}$ at the endpoints of $\Gamma_{j\pm 1}$ induce corresponding $(d_j^{\text{tov}})^{1/2}$ singularities in the boundary-data functions $G_{j,m,q}$ near the endpoints of Γ_j^{tov} , where d_j^{tov} denotes the distance from the point $x \in \Gamma_j^{\text{tov}}$ to the endpoints of Γ_j^{tov} (cf. Figure 3). Preliminary analysis indicates that, as expected, the edge singularity of the boundary data function $G_{j,m,q}$ induces additional singularities of the form $(d_j^{\text{ov}})^{-1/2}$ in the solution $\Psi_{j,m,q}$ of (3.31) as $x \in \Gamma_{j-1,j}^{\text{ov}} \cup \Gamma_{j,j+1}^{\text{ov}}$ approaches the endpoints of Γ_j^{tov} , where d_j^{ov} denotes the distance from $x \in \Gamma_{j-1,j}^{\text{ov}} \cup \Gamma_{j,j+1}^{\text{ov}}$ to the endpoints of Γ_j^{tov} . A sequence of singularities is thus set up, one density singularity resulting in a field boundary singularity which in turn induces a subsequent density singularity, resulting in a sequence of singularities given by various powers of the distances to the endpoints of Γ_j^{tov} .

These theoretical considerations together with related numerical experiments presented below suggest that all endpoint singularities encountered can be expressed in the form

$$\frac{f\left(d_p^{1/2}(x)\right)}{d_p^{1/2}(x)} \quad \text{where } f \text{ is an infinitely differentiable function} \quad (4.7)$$

in a neighborhood of each endpoint p , and where $d_p(x)$ denotes the distance from x to p . A singularity of this precise form is rigorously established in [2] for the density at a Dirichlet-Neumann junction point p ; however, a proof for the present setting remains an open question and is deferred to future work.

A numerical method designed to resolve the singular behavior just described is presented below in this section. The approach relies on a class of cosine-type changes of variables (CoV) introduced in what follows—which were originally put forth in [20, Equation (4.12)] to eliminate integrand singularities of a related but different form. These CoVs require that the non-overlapping partition Γ_{jk} of each arc Γ_j ($k = 1, 2, \dots, P_j$), as defined by the rectangular-polar discretization method [21, 22], be constructed in such a way that none of the endpoints of Γ_j or its truncated-overlap counterpart Γ_j^{tov} lie in the interior of any of the rectangular-polar patches Γ_{jk} . Further the CoVs defined below assume that the patch Γ_{jk} is parameterized by a vector function $x = x(\theta) \in \Gamma_{jk}$ with $\theta \in [-1, 1]$. In view of the discussion above and the results of this and related numerical tests, these changes variables are made an integral part of

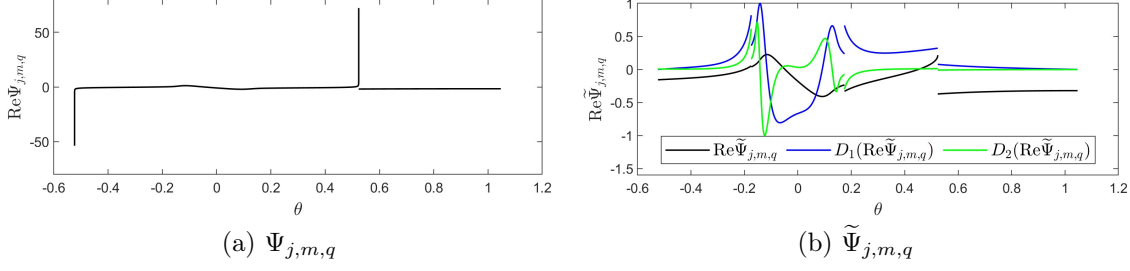


Figure 4: Comparison of the solutions $\Psi_{j,m,q}$ and $\tilde{\Psi}_{j,m,q}$ (normalized values).

the proposed numerical implementation, and, in particular, are used in all of the numerical examples presented in Section 5.

Depending on the location of the singularities of the function $\Psi_{j,m,q}$ within each rectangular-polar patch Γ_{jk} that contains such singularities, the cosine-type change of variable $\theta = \theta(s)$ ($-1 \leq s \leq 1$) for the patch Γ_{jk} used is given by

$$\theta(s) = \begin{cases} s, & \text{If no singularities exist on } \Gamma_{jk}, \\ \cos(\frac{\pi}{2}(1-s)), & \text{If singularities exist at both endpoints of } \Gamma_{jk}, \\ 1 - 2 \cos(\frac{\pi}{4}(1+s)), & \text{If a singularity exists only at the } \theta = -1 \text{ endpoint} \\ 2 \cos(\frac{\pi}{4}(1-s)) - 1, & \text{If singularity exists only at the } \theta = +1 \text{ endpoint.} \end{cases} \quad (4.8)$$

Using these change of variables we introduce the new unknown

$$\tilde{\Psi}_{j,m,q}(s) = \Psi_{j,m,q}(\theta(s))|\theta'(s)| \quad (4.9)$$

instead of $\Psi_{j,m,q}$ in (3.31) which, in particular, incorporates the Jacobian $|\theta'(s)|$.

Relying on this CoV and associated density unknown $\tilde{\Psi}_{j,m,q}(s)$, the numerical illustration that follows offers compelling evidence in support of the preceding conjecture concerning the form (4.7) of the singularities observed. This numerical example proceeds by first displaying singularities in the numerically-obtained integral densities associated with a simple multi-arc scattering problem, and by then showing that the density $\tilde{\Psi}_{j,m,q}(s)$ that results upon use of the CoV (4.8) is a smooth function, at least up to the orders of differentiation considered in the example. This clearly illustrates the assumed form (4.7) of the singularities of the density $\Psi_{j,m,q}$, since, taking into account the integration Jacobian $|\theta'(s)|$, the inverse transformations to (4.8) on a smooth density $\tilde{\Psi}_{j,m,q}(s)$ precisely induce the singularities claimed on the density $\Psi_{j,m,q}$. The numerical method is completed by utilizing the rectangular-polar method in the variable s .

For our numerical illustration we consider a scattering problem in the interior of the unit disc treated on the basis of $N = 3$ boundary open-arc patches Γ_j ($j = 1, 2, 3$), and we utilize the associated integral equation (3.31) on the arc $\Gamma_j = \{x = (\cos \theta, \sin \theta)^\top \in \mathbb{R}^2 : \theta \in (-\frac{\pi}{6}, \frac{5\pi}{6})\}$ with $j = 1$. (This is a particular case, with parameter values $\omega_0 = 2$ and $R = 1$, of the configuration called ‘‘Geometry 1’’ in Section 5.) In particular for the $j = 1$ patch we have, $\Gamma_{j-1,j}^{\text{ov}} = \{x = (\cos \theta, \sin \theta)^\top \in \mathbb{R}^2 : \theta \in (-\frac{\pi}{6}, \frac{\pi}{6})\}$ and $\Gamma_{j,j+1}^{\text{ov}} = \{x = (\cos \theta, \sin \theta)^\top \in \mathbb{R}^2 : \theta \in (\frac{\pi}{2}, \frac{5\pi}{6})\}$. The boundary data used equals the function $G_{j,m,q}$ that results from use of the multiple scattering algorithm (Algorithm 1) for $m = 5$ and $q = Q = 1$ which, in particular, contains a number of induced singularities. Figure 4(a) displays the solution $\Psi_{j,m,q}$ of equation (3.31) along the portion $\{-\frac{\pi}{6} \leq \theta \leq \frac{\pi}{3}\}$ of the $j = 1$ patch Γ_j ; the singularities of $\Psi_{j,m,q}$ near $\theta = -\frac{\pi}{6}$ and $\theta = \frac{\pi}{6}$ are clearly observed. (The density solution behaves similarly in the portion $\{\frac{\pi}{3} \leq \theta \leq \frac{5\pi}{6}\}$.) Figure 4(b), in turn, demonstrates that the solution $\tilde{\Psi}_{j,m,q}$ is smooth, at least up to the orders of differentiation considered, and thus provides the desired numerical evidence of conjectured singularity structure of the solution $\Psi_{j,m,q}$.

5 Numerical results

This section presents a variety of numerical results, produced by means of the FTH-MS integral equation solver introduced in this paper, which illustrate the efficiency and accuracy of the proposed methods. With reference to Section 4.1, we denote by $\mathcal{F} = \{\omega_1, \dots, \omega_J\}$ a set of frequencies used for the Fourier transformation process, which includes equi-spaced grids in the frequency intervals $[-W, -w_c]$ and $[w_c, W]$, as well as Clenshaw-Curtis mesh points in the intervals $(-\mu_{j+1}, -\mu_j)$ and (μ_j, μ_{j+1}) , $j = 1, \dots, P$. For the necessary time-domain discretization, in turn, we use the mesh $\mathcal{T} = \{t_n = n\Delta t\}_{n=1}^{N_T}$ of the time interval $[0, s_Q + H]$ (cf. eq. (2.13)), where $\Delta t = (s_Q + H)/N_T$. In regard to the time windowing strategy, in turn, we set $H = 10$, $s_q = \frac{3}{2}(q-1)H$, $q \in \mathcal{Q}$, and

$$\square_q(t) = \square(t - s_q), \quad \square(s) = \begin{cases} \eta(s/H; 1/2, 1), & -H/2 \leq s \leq H, \\ 1 - \eta(s/H + 3/2; 1/2, 1), & -H < s < -H/2, \\ 0, & |s| \geq H, \end{cases}$$

where the function η is defined in (3.3). For simplicity, with exception of the long-time propagation problem illustrated in Figure 7, all of the numerical examples presented in this paper utilize the value $Q = 1$ (single incident-field window). Sufficiently fine frequency-independent meshes are used on the boundaries Γ_j , $j = 1, \dots, N$ for all frequencies considered, where, in accordance with Section 4.2, the open-arc integral equations (3.31) are numerically solved using the Chebyshev-based rectangular-polar solver described in Section 4.3, while the closed-curve integral equations (3.34) are solved using the Nyström method [24]. The numerical errors ε presented in this section were calculated in accordance with the expression

$$\varepsilon = \max_{t \in [0, T]} |u_{\text{num}}^s - u_{\text{ref}}^s| \quad (5.1)$$

where, with exception of the test cases considered in connection with Geometries 3 and 6, for which the closed-form solutions are known, the reference solutions u_{ref}^s were obtained as numerical solutions produced by means of sufficiently fine discretizations. All of the numerical results presented in this paper were obtained on the basis of C++ numerical implementations of the algorithms described in the previous sections, parallelized using OpenMP, and run on a 8-core Lenovo Laptop with an AMD Core processor R7-8845H.

Four different types of incident fields are considered in this section (all of which are solutions of the wave equation), namely

1. A Gaussian-modulated point source $u_1^i(x, t)$ equal to the Fourier transform of the function

$$U_1^i(x, \omega) = \frac{5i}{2} H_0^{(1)}(\omega|x - z_0|) e^{-\frac{(\omega - \omega_0)^2}{\sigma^2}} e^{i\omega\tau_0} \quad (5.2)$$

with respect to ω , with $\sigma = 2$ and $\tau_0 = 4$;

2. A Gaussian-modulated plane-wave incidence $u_2^i(x, t)$ equal to the Fourier transform of the function

$$U_2^i(x, \omega) = e^{i\omega x \cdot d^{\text{inc}}} e^{-\frac{(\omega - \omega_0)^2}{\sigma^2}} e^{i\omega\tau_0} \quad (5.3)$$

with respect to ω , with $\sigma = \sqrt{2}$, $\tau_0 = 6$, and with incident direction vector $d^{\text{inc}} = (\cos \theta^{\text{inc}}, \sin \theta^{\text{inc}})^\top$;

3. A pulse plane-wave incident field

$$u_3^i(x, t) = -\sin(4\ell(x, t)) e^{-1.6(\ell(x, t) - 3)^2}, \quad \ell(x, t) = t - t_{\text{lag}} - x \cdot d^{\text{inc}} \quad (5.4)$$

along the incident direction $d^{\text{inc}} = (\cos \theta^{\text{inc}}, \sin \theta^{\text{inc}})^\top$ with $t_{\text{lag}} = 2$; and

4. The multi-pulse incident field

$$u_4^i = \sum_{j=0}^4 u_3^i(x, t - 10j). \quad (5.5)$$

On the basis of these incident fields, a variety of numerical examples are presented in what follows for five different scattering geometries, as described below.

Geometry 1. The domain D in this case equals the disc of radius $R > 0$ centered at the origin. Equi-sized overlapping patches are selected such that $\delta_{\min} \approx 0.35$ for $R = 1$, $N = 3$ and $\delta_{\min} \approx 0.42$ for $R = 2$, $N = 6$, where δ_{\min} is defined in (3.4). Interior wave equation problems for two different time-domain incident fields, namely, the plane wave $u_2^i(x, t)$ and the multi-pulse incident field u_4^i , are considered for this geometry. For the plane wave $u_2^i(x, t)$ incidence, the fixed numerical frequency interval $\omega \in [5, 25]$ is used for the necessary numerical Fourier transformation, and the parameter values $\theta^{inc} = 0$, $\omega_0 = 15$, $J = 501$ and $\Delta t = 0.01$ were set. For the multi-pulse incident field u_4^i , in turn, for which a long time propagation problem is considered in what follows, the parameter values $W = 20$, $J = 872$, $\Delta t = 0.1$, and $M = 40$ were used. For both the plane-wave and multi-pulse incidence test cases the exact solutions are given by $u(x, t) = -u_2^i(x, t)$ and $u(x, t) = -u_4^i(x, t)$ for $x \in D$, respectively. Solution values and numerical errors for various values of M at $x = (0.5, 0)^\top$ as a function of t resulting for the problems with plane wave $u_2^i(x, t)$ incidence are displayed in Figures 5–6: clearly, high accuracy and rapid convergence with respect to M are observed. The numerical and exact solutions at $x = (0.5, 0)^\top$ for the case of $u_4^i(x, t)$ incidence are displayed in Figure 7; the errors in the numerical solution displayed are uniformly less than 10^{-6} .

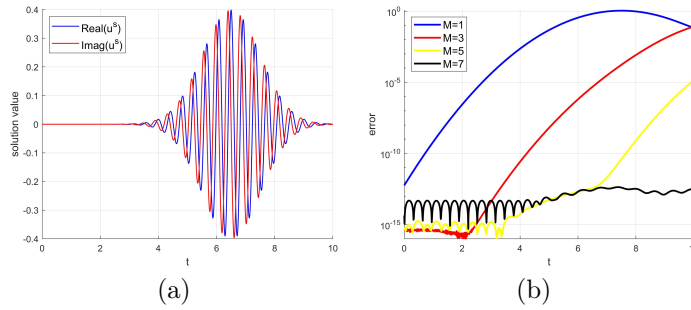


Figure 5: Scattered field and errors obtained for the problem considered in Geometry 1 with $R = 1$ and $N = 3$. (a) Real and imaginary parts of scattered field at $x = (0.5, 0)^\top$ resulting from the incident field u_2^i . (b) Numerical errors as functions of time t for various values of M .

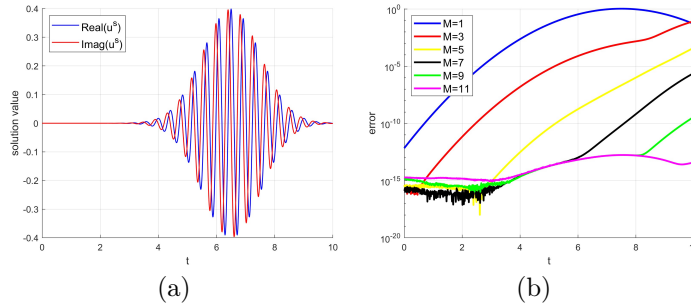


Figure 6: Scattered field and errors obtained for the problem considered in Example 1 with $R = 2$ and $N = 6$. (a) Real and imaginary parts of scattered field at $x = (0.5, 0)^\top$ resulting from the incident field u_2^i . (b) Numerical errors as functions of time t for various values of M .

Geometry 2. Scattering problems in the interior of a complex H-shaped domain centered at the origin are considered next, utilizing the point source incidence function u_1^i with $z_0 = (0, 0)$ and with two different frequencies: $\omega_0 = 15$ and $\omega_0 = 50$. The Fourier-transforms utilized to produce the corresponding time-domain incident-fields (which are necessary to obtain the total time-domain fields $u^{\text{tot}} = u^i + u$ displayed

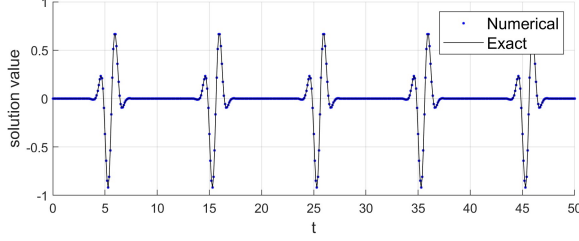


Figure 7: Long-time propagation illustration. Real parts of the numerical and exact solutions at $x = (0.5, 0)^\top$ resulting from the incident field u_4^i .

in Figure 8) were evaluated by integrating in the frequency ranges $[5, 25]$ and $[40, 60]$ respectively—outside which the frequency-domain incident fields are vanishingly small. The parameter values $N = 4$, $J = 501$, $\Delta t = 0.01$ and $M = 10$ were used. Figure 8 displays the total field u^{tot} within D at various times.

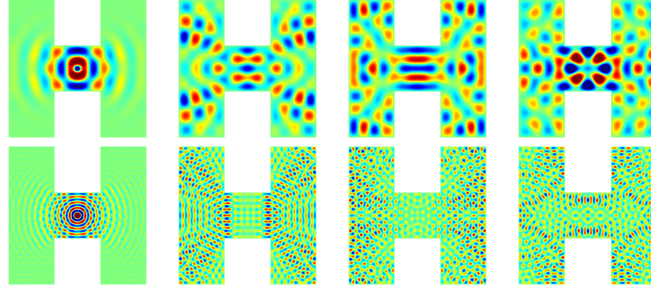


Figure 8: Real part of the total field u^{tot} for the problems of scattering associated with the Geometry 2, with point source u_1^i located at $z_0 = (0, 0)^\top$. Upper row: $w_0 = 15$, Lower row: $w_0 = 50$. Fields at time $t = 4, 6, 8$ and 10 are displayed from left to right in each row.

Geometries 3. Problems of scattering posed in the exterior of the groups of obstacles depicted in Figures 9(a) and 10(a) are now considered, with incident fields given by the functions u_1^i and u_2^i . For the incident function u_1^i the point z_0 is located within one of the obstacles, and, therefore, the exact solution for the problem is given by $u(x, t) = -u_1^i(x, t)$ for $x \in D^e$. The numerical errors as a function of t for various values of M are displayed in Figures 9 and 10 which clearly demonstrate the high accuracy of the proposed solver. Figure 11 displays the numerical total field resulting from the scattering of the plane incidence u_2^i for various values of θ^{inc} . The parameter values $\omega_0 = 15$, $W = 25$, $J = 800$ and $\Delta t = 0.0125$ were used for all of the Geometry 3 cases.

Geometry 4. We now consider scattering problems in the exterior of the group of three open-arcs displayed in Figure 12(a). A point source u_1^i with $z_0 = (0, 0)^\top$ and $\omega_0 = 15$ is considered for this example, for which we used the parameter values $W = 25$, $J = 800$ and $\Delta t = 0.0125$. The resulting numerical errors as a function of t for various values of M are presented in Figure 12 which also demonstrates the high accuracy of the proposed solver. The numerical total fields resulting for this geometry from the scattering of the plane incidence u_2^i with $\theta^{\text{inc}} = -\frac{3}{4}\pi$ are displayed in Figure 13.

Geometries 5. Finally we consider problems of scattering by a highly trapping open-arc cavity structures with a small openings, whose numerical solution can be challenging on account of wave trapping and associated large numbers of GMRES frequency-domain iterations. We consider two cavity geometries, namely, a circular cavity $\Gamma = \{x = (\cos \theta, \sin \theta)^\top \in \mathbb{R}^2 : \theta \in (0.02\pi, 1.98\pi)\}$ and a rocket-like open cavity (see Figure 17) for which we choose $N = 6$ and $N = 10$, respectively. We first consider the problem of a circular cavity under plane wave incidence, $u_2^i(x, t)$, with an incidence angle $\theta^{\text{inc}} = -\pi$,

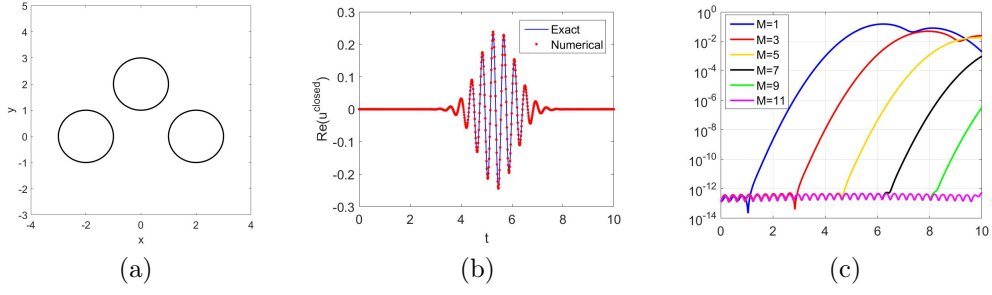


Figure 9: Real part of the scattered field (b) at $x = (-1, 1)^\top$ resulting from the incident field u_1^i with $z_0 = (0, 2)^\top$ and numerical errors (c) as functions of time t for various values of M obtained for the exterior wave equation problem with 3 bounded obstacles (a) considered in Geometry 3.

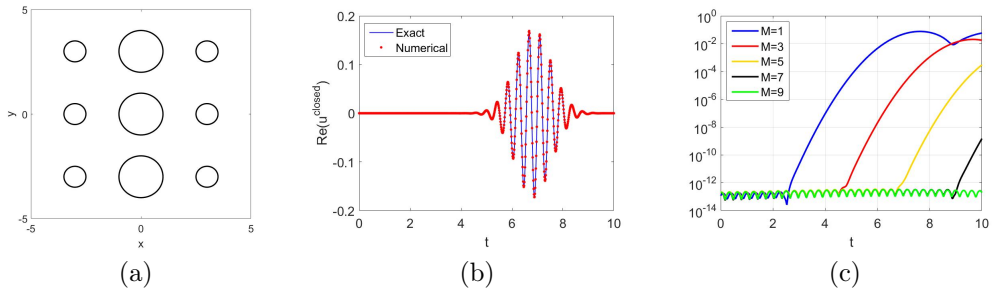


Figure 10: Real part of the scattered field (b) at $x = (2, 2)^\top$ resulting from the incident field u_1^i with $z_0 = (0, 0)^\top$ and numerical errors (c) as functions of time t for various values of M obtained for the exterior wave equation problem with 9 bounded obstacles (a) considered in Geometry 3.

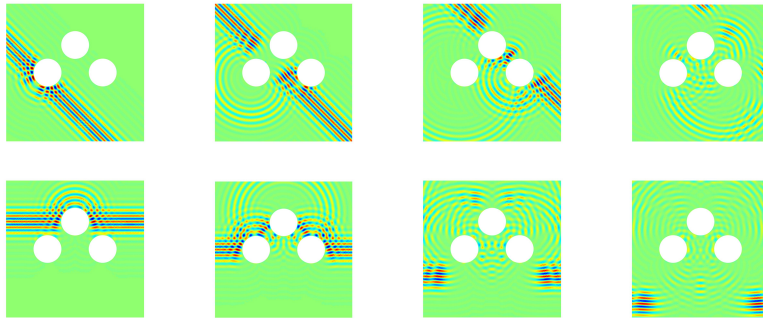


Figure 11: Real part of the total fields for the scattering of plane incidence u_1^i by three bounded obstacles considered in Geometry 3. Upper row: $\theta^{\text{inc}} = \frac{\pi}{4}$. Lower row: $\theta^{\text{inc}} = -\frac{\pi}{2}$. Fields at times $t = 2, 4, 6$ and 8 are displayed from left to right in each row.

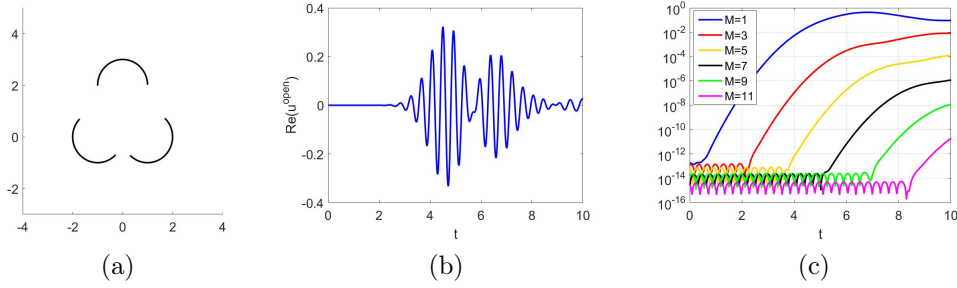


Figure 12: Real part of the scattered field (b) at $x = (-1, 0)^\top$ resulting from the incident field u_2^i and numerical errors (c) as functions of time t for various values of M obtained for the exterior wave equation problem with 3 open-arcs (a) considered in Geometry 4.

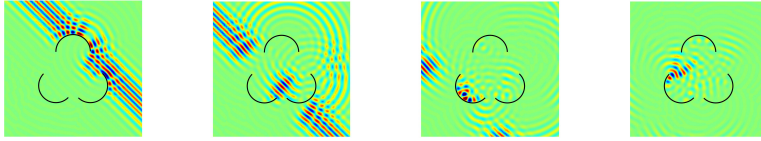


Figure 13: Real part of the total fields for the scattering of plane wave u_2^i with $\theta^{\text{inc}} = -\frac{3}{4}\pi$ by three open-arcs considered in Geometry 4. Fields at times $t = 2, 4, 6$ and 8 are displayed from left to right.

and using the parameter values: $\omega_0 = 15$, $W = 25$, $J = 401$, and $\Delta t = 0.01$. Solution values at $x = (-0.5, 0)^\top$ as a function of t together with numerical errors resulting for various values of M are displayed in Figure 14. The total fields for the higher-frequency case $\omega_0 = 50$ are displayed in Figure 15. We emphasize the substantial benefits of boundary decomposition, which, as illustrated in Figure 16, can significantly reduce the number of GMRES iterations required for the numerical evaluation of the frequency-domain BIEs. The total fields for the rocket-like open cavity under the $u_2^i(x, t)$ incident field with $\omega_0 = 50$ and $M = 50$ are presented in Figure 17.

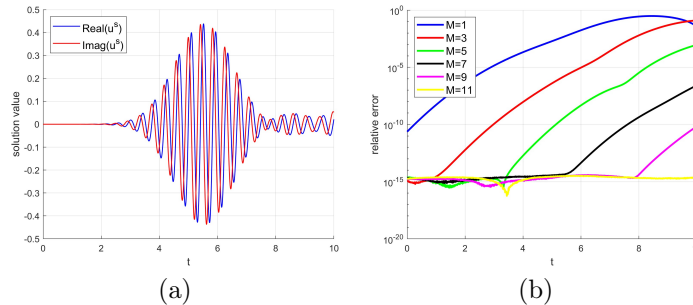


Figure 14: Real part of the scattered field (a) at $x = (0.5, 0)^\top$ resulting from the incident field u_2^i with $\theta^{\text{inc}} = -\pi$. and numerical errors (b) as functions of time t for various values of M .

6 Concluding remarks

In significant extension of a previous two-patch interior multiple-scattering wave equation solver [22], and on the basis of a newly introduced spatially-windowed multi-patch decomposition strategy, this paper proposed new multi-patch multiple-scattering FTH-MS methodologies for the solution of both interior

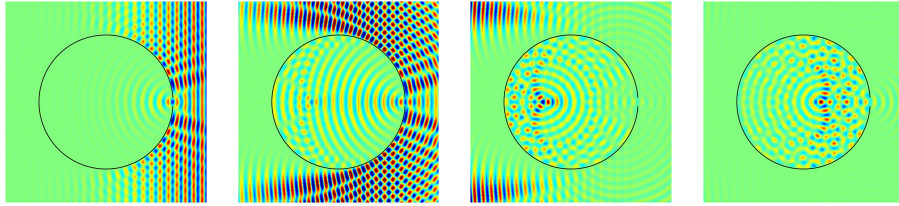


Figure 15: Real part of the total fields for the scattering of plane wave u_2^i with $\theta^{\text{inc}} = -\pi$ by considered in Example 5. Fields at times $t = 4, 6, 8$ and 10 are displayed from left to right.

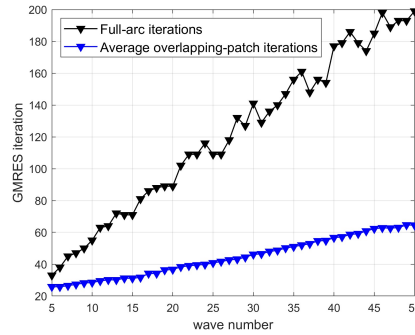


Figure 16: GMRES iteration numbers for different frequencies while solving the integral equation (3.31) on the full-arc (circular cavity) or 6 overlapping patches such that the relative residual is smaller than 10^{-6} .

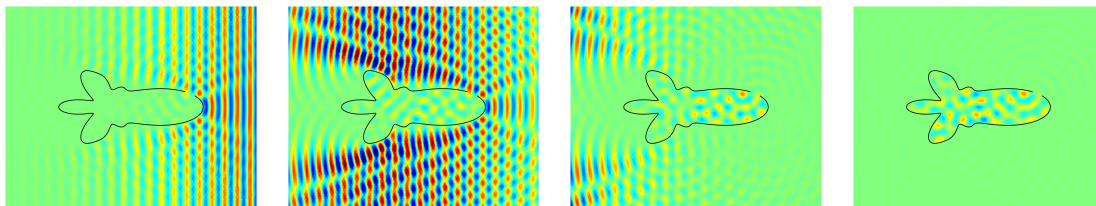


Figure 17: Real part of the total fields for the scattering of plane wave u_2^i with $\theta^{\text{inc}} = -\pi$ by rocket-like open cavity. Fields at times $t = 4, 6, 8$ and 10 are displayed from left to right.

and exterior wave equation problems. In particular, on the basis of the Huygens-like domain-of-influence condition, this paper established rigorously that the sum of the overlapping-arc multiple scattering solutions coincides with the solution to the original wave equation problem. Two key innovations distinguish the present contribution from the previous multi-scattering method [22], namely (i) The use of a POU along the boundary now enables the treatment of an arbitrary number of overlapping arcs, whereas the earlier algorithm was limited to a maximum of two; and (ii) The new change-of-variables-based handling of density singularities arising from the overlapping-arc method replaces the ad-hoc technique used in [22]—which, relying on extension of the scatterer boundaries along the normal direction, is rather cumbersome and fails in the presence of open arcs on the scattering surface. In all cases the solver transforms the original problem into a sequence of scattering problems involving the given overlapping open arcs and closed curves, each one of which is solved on the basis of the “smooth time-windowing and recentering” methodology and high-frequency Fourier transform algorithms [6]. The solves required for the sequence of smooth temporal windows can clearly be performed in parallel, allowing for implementations that leverage parallelization of the time evolution. As demonstrated through various numerical examples, the proposed methodologies enable long-time simulations, including incident signals of extended duration, while maintaining high accuracy and negligible dispersion errors. The extension of these ideas to three-dimensional problems, as well as their application to elastic and electromagnetic wave phenomena and multi-layered media, is left for future work.

Acknowledgments

This work is partially supported by the National Key R&D Program of China, Grants No. 2024YFA1016000 and 2023YFA1009100, the Strategic Priority Research Program of the Chinese Academy of Sciences, Grant No. XDB0640000, the Key Project of Joint Funds for Regional Innovation and Development (U21A20425) Province, NSFC under grants 12171465 and a Key Laboratory of Zhejiang Province. OB gratefully acknowledges support for NSF and AFOSR under contracts DMS-2109831, FA9550-21-1-0373 and FA9550-25-1-0015.

References

- [1] A. Aimi, M. Diligenti, C. Guardasoni, On the energetic Galerkin boundary element method applied to interior wave propagation problems, *J. Comput. Appl. Math.* 235(7) (2011) 1746-1754.
- [2] E. Akhmetgaliyev and O. Bruno, Regularized integral formulation of mixed Dirichlet-Neumann problems, *Journal of Integral Equations and applications* 29 (2017) 493-529.
- [3] B. Alpert, L. Greengard, T. Hagstrom, Nonreflecting boundary conditions for the time-dependent wave equation, *J. Comput. Phys.* 180 (2002) 270-296.
- [4] F. Amlani, O. P. Bruno, An FC-based spectral solver for elastodynamic problems in general three-dimensional domains, *J. Comput. Phys.* 307 (2016) 333-354.
- [5] T.G. Anderson and O. P. Bruno, “Bootstrap Domain of Dependence”: Bounds and Time Decay of Solutions of the Wave Equation, arXiv preprint arXiv:2010.09002 (2022) .
- [6] T.G. Anderson, O. P. Bruno, M. Lyon, High-order, dispersionless “fast-hybrid” wave equation solver. Part I: $O(1)$ sampling cost via incident-field windowing and recentering, *SIAM J. Sci. Comput.* 422 (2020) A1348-A1379.
- [7] T.G. Anderson, O. P. Bruno, M. Lyon, Fast Hybrid wave equation solver Part II: 3D window tracking, 2D asymptotics tracking, general incident fields and remote field evaluation, In preparation.
- [8] I.M. Babuška, S.A. Sauter, Is the pollution effect of the FEM avoidable for the Helmholtz equation considering high wave numbers? *SIAM J. Numer. Anal.* 34 (1997) 2392-2423.

- [9] A. Bamberger, T. Ha-Duong, Formulation variationnelle espace-temps pour le calcul par potentiel retardé de la diffraction d'une onde acoustique, *Math. Methods Appl. Sci.* 8 (1986) 405-435.
- [10] L. Banjai, M. Kachanovska, Fast convolution quadrature for the wave equation in three dimensions, *J. Comput. Phys.* 279 (2014) 103-126.
- [11] P. Bansal, A. Moiola, I. Perugia, C. Schwab, Space-time discontinuous Galerkin approximation of acoustic waves with point singularities, *IMA J. Numer. Anal.* 41 (2021) 2056-2109.
- [12] A.H. Barnett, L. Greengard, T. Hagstrom, High-order discretization of a stable time-domain integral equation for 3D acoustic scattering, *J. Comput. Phys.* 402 (2020) 109047.
- [13] C. Bauinger, O.P. Bruno, "Interpolated Factored Green Function" method for accelerated solution of scattering problems, *J. Comput. Phys.* 430 (2021) 110095.
- [14] J.-P. Berenger, A perfectly matched layer for the absorption of electromagnetic waves, *J. Comput. Phys.* 114 (1994) 185-200.
- [15] O.P. Bruno, M. Lyon, C. Pérez-Arancibia, C. Turc, Windowed Green function method for layered-media scattering, *SIAM J. Appl. Math.* 76(5) (2016) 1871-1898.
- [16] O.P. Bruno, E. Garza, A Chebyshev-based rectangular-polar integral solver for scattering by general geometries described by non-overlapping patches, *J. Comput. Phys.* 421 (2020) 109740.
- [17] O.P. Bruno, E. Garza, C. Pérez-Arancibia, Windowed Green function method for nonuniform open-waveguide problems, *IEEE Trans. Antenn. Propag.* 65 (2017) 4684-4692.
- [18] O.P. Bruno, S. Lintner, Second-kind integral solvers for TE and TM problems of diffraction by open arcs, *Radio Sci.* 47 (6) (2012).
- [19] O.P. Bruno, M. Lyon, High-order unconditionally stable FC-AD solvers for general smooth domains I. Basic elements, *J. Comput. Phys.* 229 (6) (2010) 2009-2033.
- [20] O.P. Bruno, T. Yin, Regularized integral equation methods for the elastic scattering problems in three dimensions, *J. Comput. Phys.* 410 (2020) 109350.
- [21] O.P. Bruno, T. Yin, A windowed Green function method for elastic scattering problems on a half-space, *Comput. Methods Appl. Mech. Engrg.* 376 (2021) 113651.
- [22] O.P. Bruno, T. Yin, Multiple-scattering frequency-time hybrid solver for the wave equation in interior domains, *Math. Comput.* 93(346) (2024) 551-587.
- [23] Q. Chen, H. Haddar, A. Lechleiter, P. Monk, A sampling method for inverse scattering in the time domain, *Inverse Problems* 8 (2010) 85001-85017.
- [24] D. Colton and R. Kress, *Inverse Acoustic and Electromagnetic Scattering Theory*, Berlin, Springer, 1998.
- [25] M. Costabel, M. Dauge, R. Duduchava, Asymptotics without logarithmic terms for crack problems, *Commun. Partial Differ. Equ.* 28 (2003) 869-926.
- [26] J. Douglas, J.E. Santos, D. Sheen, L.S. Bennethum, Frequency domain treatment of one-dimensional scalar waves, *Math. Models Methods Appl. Sci.* 3 (1993) 171-194.
- [27] T. Ha-Duong, On retarded potential boundary integral equations and their discretisation, in *Topics in Computational Wave Propagation: Direct and Inverse Problems*, M. Ainsworth et al., eds., Springer Berlin Heidelberg, Berlin, Heidelberg, 2003, pp. 301-336.

- [28] B. Engquist, A. Majda, Absorbing boundary conditions for the numerical simulation of waves, *Math. Comp.* 31 (1977) 629–629.
- [29] L.C. Evans, *Partial Differential Equations* (2nd edition), Graduate Studies in Mathematics, Vol. 19, American Mathematical Society, Providence, 2010.
- [30] D.A. French, T.E. Peterson, A continuous space-time finite element method for the wave equation, *Math. Comp.* 65 (1996) 491-506.
- [31] M.J. Grote, A. Schneebeli, D. Schötzau, Discontinuous Galerkin finite element method for the wave equation, *SIAM J. Numer. Anal.* 44 (2006) 2408-2431.
- [32] M. Hassell, T. Qiu, T. Sánchez-Vizuet, F.-J. Sayas, A new and improved analysis of the time domain boundary integral operators for acoustics, *J. Integral Equations Applications* 29(1) (2017) 107-136.
- [33] I. Labarca, R. Hiptmair, Acoustic scattering problems with convolution quadrature and the method of fundamental solutions, *Commun. Comput. Phys.* 30 (2021) 985-1008.
- [34] A.R. Laliena, F.-J. Sayas, Theoretical aspects of the application of convolution quadrature to scattering of acoustic waves, *Numer. Math.* 112 (2009) 637-678.
- [35] Y. Liu, *Fast Multipole Boundary Element Method*, Cambridge University Press, New York, 2009.
- [36] R. Löscher, O. Steinbach, M. Zank, Numerical results for an unconditionally stable space-time finite element method for the wave equation, *Domain Decomposition Methods in Science and Engineering XXVI*, 625-632.
- [37] C. Lubich, On the multistep time discretization of linear initial-boundary value problems and their boundary integral equations, *Numer. Math.* 67 (1994) 365-389.
- [38] R. C. MacCamy, Low frequency acoustic oscillations, *Q. Appl. Math.* 23 (1965) 247-255.
- [39] E. Mecocci, L. Misici, M. C. Recchioni, F. Zirilli, A new formalism for time-dependent wave scattering from a bounded obstacle, *J. Acoust. Soc. Am.* 107 (2000) 1825-1840.
- [40] J. M. Melenk and S. Sauter, Wavenumber explicit convergence analysis for galerkin discretizations of the helmholtz equation, *SIAM J. Numer. Anal.* 49 (2011) 1210–1243.
- [41] F.-J. Sayas, *Retarded Potentials and Time Domain Boundary Integral Equations*, Springer International Publishing, 2016.
- [42] J. Shen and T. Tang, *Spectral and High-Order Methods with Applications*, Beijing Science Press, 2006.
- [43] E.P. Stephan, W.L. Wendland, An augmented Galerkin procedure for the boundary integral method applied to two-dimensional screen and crack problems, *Appl. Anal.* 3 (1984) 183-219.
- [44] O. Steinbach, C. Urzúa-Torres, A new approach to space-time boundary integral equations for the wave equation, *SIAM J. Math. Anal.* 54(2) (2022) 1370-1392.
- [45] O. Steinbach, C. Urzúa-Torres, M. Zank, Towards coercive boundary element methods for the wave equation, [arXiv:2106.01646](https://arxiv.org/abs/2106.01646).
- [46] J.A. Stratton, *Electromagnetic theory*, McGraw-Hill, New York, 1941.
- [47] Z. Sun, Y. Xing, Optimal error estimates of discontinuous Galerkin methods with generalized fluxes for wave equations on unstructured meshes, *Math. Comput.* 90 (2021) 1741-1772.

- [48] A. Taflove, Computational electrodynamics: the finite-difference time-domain method, Artech House, Boston, 2000.
- [49] P. Werner, Low frequency asymptotics for the reduced wave equation in two-dimensional exterior spaces, *Math. Meth. Appl. Sci.* 8 (1986): 134-156.
- [50] Y. Xing, C.-S. Chou, C.-W. Shu, Energy conserving local discontinuous Galerkin methods for wave propagation problems, *Inverse Probl. Imag.* 7 (2013) 967-986.
- [51] Y. Yue, F. Ma, B. Chen, Time domain linear sampling method for inverse scattering problems with cracks, *E. Asian J. Appl. Math.* 12(1) (2022) 96-110.